Environmental Research 166 (2018) 348–362

Contents lists available at ScienceDirect

Environmental Research

journal homepage: www.elsevier.com/locate/envres

Alzheimer's disease and alpha-synuclein pathology in the olfactory bulbs of infants, children, teens and adults ≤ 40 years in Metropolitan Mexico City. APOE4 carriers at higher risk of suicide accelerate their olfactory bulb pathology

Lilian Calderón-Garcidueñas[a,b,*], Angélica González-Maciel[c], Rafael Reynoso-Robles[c], Randy J. Kulesza[d], Partha S. Mukherjee[e], Ricardo Torres-Jardón[f], Topi Rönkkö[g], Richard L. Doty[h]

[a] The University of Montana, Missoula, MT, 59812, USA
[b] Universidad del Valle de México, 14370, Mexico
[c] Instituto Nacional de Pediatría, Mexico City, 04530, Mexico
[d] Auditory Research Center, Lake Erie College of Osteopathic Medicine, Erie, PA 16509, USA
[e] Mathematics Department, Boise State University, Boise, ID 83725, USA
[f] Centro de Ciencias de la Atmósfera, Universidad Nacional Autónoma de México, 04310, Mexico
[g] Aerosol Physics, Faculty of Natural Sciences, Tampere University of Technology, FI-33101 Tampere, Finland
[h] Smell and Taste Center, Department of Otorhinolaryngology: Head and Neck Surgery, Perelman School of Medicine, University of Pennsylvania, 19104, USA

ARTICLE INFO

Keywords:
Alzheimer
Alpha synuclein
Alpha-synucleinopathies
Amyloid plaques
Air pollution
APOE4
Children
Corpora amylacea
Combustion-derived nanoparticles CDNPs
Hyperphosphorylated tau
Mexico City
Nanocluster aerosol particles
Olfactory bulb
Parkinson
$PM_{2.5}$
Suicide
Tauopathies
Young adults

ABSTRACT

There is growing evidence that air pollution is a risk factor for a number of neurodegenerative diseases, most notably Alzheimer's (AD) and Parkinson's (PD). It is generally assumed that the pathology of these diseases arises only later in life and commonly begins within olfactory eloquent pathways prior to the onset of the classical clinical symptoms. The present study demonstrates that chronic exposure to high levels of air pollution results in AD- and PD-related pathology within the olfactory bulbs of children and relatively young adults ages 11 months to 40 years. The olfactory bulbs (OBs) of 179 residents of highly polluted Metropolitan Mexico City (MMC) were evaluated for AD- and alpha-synuclein-related pathology. Even in toddlers, hyperphosphorylated tau (hTau) and Lewy neurites (LN) were identified in the OBs. By the second decade, 84% of the bulbs exhibited hTau (48/57), 68% LNs and vascular amyloid (39/57) and 36% (21/57) diffuse amyloid plaques. OB active endothelial phagocytosis of red blood cell fragments containing combustion-derived nanoparticles (CDNPs) and the neurovascular unit damage were associated with myelinated and unmyelinated axonal damage. OB hTau neurites were associated mostly with pretangle stages 1a and 1b in subjects ≤ 20 years of age, strongly suggesting olfactory deficits could potentially be an early guide of AD pretangle subcortical and cortical hTau. APOE4 versus APOE3 carriers were 6–13 times more likely to exhibit OB vascular amyloid, neuronal amyloid accumulation, alpha-synuclein aggregates, hTau neurofibrillary tangles, and neurites. Remarkably, APOE4 carriers were 4.57 times more likely than non-carriers to die by suicide. The present findings, along with previous data that over a third of clinically healthy MMC teens and young adults exhibit low scores on an odor identification test, support the concept that olfactory testing may aid in identifying young people at high risk for neurodegenerative diseases. Moreover, results strongly support early neuroprotective interventions in fine particulate matter ($PM_{2.5}$) and CDNP's exposed individuals ≤ 20 years of age, and the critical need for air pollution control.

1. Introduction

Urban polluted environments and occupational exposures with ubiquitous high concentrations of ultrafine particles (UFP, diameter < 100 nm) (Zhu et al., 2002; Pirjola et al., 2016), nanoparticles (NP, diameter < 100 nm), and the recently discovered nanocluster aerosol particles (NCA, diameter < 3.0 nm) (Rönkkö et al., 2017) emitted by road transportation are of great concern for the nervous system due to their high potential to penetrate biological barriers, including vascular endothelium, alveolar-capillary, olfactory, nasal,

* Corresponding author at: University of Montana, 32 Campus Drive, 287 Skaggs Building, Missoula, MT 59812, USA.
E-mail address: lilian.calderon-garciduenas@umontana.edu (L. Calderón-Garcidueñas).

https://doi.org/10.1016/j.envres.2018.06.027
Received 7 May 2018; Received in revised form 12 June 2018; Accepted 12 June 2018

gastrointestinal, blood-brain-barrier (BBB) and blood-CSF barrier (Maher et al., 2016; González-Maciel et al., 2017; Calderón-Garcidueñas et al., 2018). Combustion aerosol particle sources, i.e., vehicles powered with internal combustion engines and combustion-based production of heat and power, are frequently situated closed to people increasing their relative importance in respect of human exposures to particulate matter (PM). Combustion-originated particles are composed of elemental carbon, organic and sulfuric compounds and metals (Enroth et al., 2016; Mylläri et al., 2017; Rönkkö et al., 2014) found in fuels, lubricant oils and engine wear. Iron and associated transition metals of NPs are highly oxidative and strongly magnetic (Maher et al., 2016). The entire range of very small particles gain entry to the brain in significant amounts in children, and young adult Metropolitan Mexico City (MMC) residents and are known to cause severe damage to critical cellular organelles in the central nervous system (CNS) (Calderón-Garcidueñas et al., 2016a, 2017; González-Maciel et al., 2017).

Exposure to air pollutants appear to play a major role in the development and/or acceleration of Alzheimer's disease (AD) (Calderón-Garcidueñas et al., 2002, 2008a, 2008b; González-Maciel et al., 2017; Jung et al., 2015; Maher et al., 2016; Chen et al., 2017; Marabotti et al., 2017). MMC residents who live under high levels of air pollution show an early brain imbalance in genes involved in oxidative stress, inflammation, and innate and adaptive immune responses (Calderón-Garcidueñas et al., 2012). Dysregulated neuroinflammation, diffuse brain neurovascular unit damage, and the accumulation of misfolded proteins associated with the early stages of both AD and Parkinson's disease (PD) are seen in MMC residents, but not in individuals coming from regions of low air pollution (Calderón-Garcidueñas et al., 2003, 2007b, 2008b, 2010, 2011, 2012, 2016a, 2016b, 2017). Olfactory dysfunction is a hallmark of these disorders, occurring long before the onset of their clinical phenotypic manifestations (Doty, 2012, 2017). Because of this fact, and evidence that nanoparticles and other components of air pollution can enter into the nose, bypass the blood brain barrier, and penetrate the brain via the olfactory receptor cells and perineural spaces, the olfactory bulbs (OBs) have become a primary focus for understanding the relationship between air pollution and neurodegenerative disease pathology (Doty, 2008). The OBs clearly participate in the brisk neuroinflammatory process related to exposures to polluted air where particulate matter and metals are key components, along with endotoxins and CDNPs (Bravo-Alvarez and Torres-Jardón, 2002; Vega et al., 2010; Molina et al., 2010; Aiken et al., 2009; Marr et al., 2006; Querol et al., 2008; Calderón-Garcidueñas et al., 2013).

We have previously described the association between olfactory bulb apurinic/apyrimidinic (AP) lesion sites in genomic DNA and the presence of metals like Ni and V (from industrial environmental sources). A pathologic gradient was identified (olfactory mucosa > olfactory bulb > frontal cortex) which included significant OB neuroinflammation and upregulation of IL1β and COX2 in MMC residents (Calderón-Garcidueñas et al., 2003, 2013). The clinical counterpart was seen in MMC children (13.4 ± 4.8 years, 28 APOE 3 and 22 APOE 4), where the failure of APOE4 children to identify the soap odor in the University of Pennsylvania Smell Identification Test (UPSIT) was correlated with a higher mI/Cr ratio in the left hippocampus (Calderón-Garcidueñas et al., 2015). Earlier, we demonstrated OB pathology in a cohort of 35 MMC vs 9 control subjects ages 20.8 ± 8.5 years assessed by light and electron microscopy (Calderón-Garcidueñas et al., 2010). MMC residents showed, with no exceptions, OB vascular changes, neuronal accumulation of particles, and/or immunoreactivity (IR) to beta amyloid and/or alpha-synuclein in neurons, glial cells, and/or blood vessels. CDNPs were documented in the endothelial cytoplasm and basement membranes of the OBs. In contrast to Mexico City olfactory bulb extensive pathology, the OBs from clean air control residents were unremarkable (Calderón-Garcidueñas et al., 2010). In the same work we also described the results of the UPSIT administration to 62 MMC v 25 controls age 21.2 ± 2.7 years. Olfaction deficits were present in 35.5% MMC and 12% of controls (Calderón-Garcidueñas et al., 2010). Of considerable interest was the observation that APOE 4 carriers failed 2.4 ± 0.54 items in the 10-item smell identification scale from the UPSIT related to Alzheimer's disease, while APOE 2/3 and 3/3 subjects failed 1.36 ± 0.16 items, a highly significant result p = 0.01 (Calderón-Garcidueñas et al., 2010).

In this study we documented, using immunohistochemistry, the early stages of AD- and α-synuclein-related olfactory bulb pathology in young persons living in highly polluted regions of MMC. We employed electron microscopy to document vascular pathology and to identify and measure the sizes of combustion-derived nanoparticles and the associated organelle pathology within the bulbs. Our laboratory is particularly interested in the progression of olfactory bulb pathology with age and cumulative exposures to fine particulate matter ($PM_{2.5}$) above the USEPA standard (primary: 12 μg/m^3, annual mean averaged over 3 years). Identifying key air pollutants, composition and sizes of nanoparticles, and other factors that impact early neural risk within the olfactory system and its interrelated CNS structures has the potential to allow for modifying the course of AD and PD during their genesis early in life.

2. Methods

2.1. Study design and samples

One hundred and seventy-nine consecutive autopsies with sudden causes of death that it did not involve the brain were selected for this study. MMC subjects ages 11 months to 40 years were clinically healthy prior to their sudden demise and were included in this study if:

(a). Sections of olfactory bulb contained the anterior olfactory nucleus, granular, plexiform and glomerular layers and olfactory tract white matter, (b). Gross examination of the brain was unremarkable, and (c). Macro and microscopic examination of extra-neural key organs was unremarkable. Examination of autopsy materials was approved by the Forensic Institute in Mexico City. Autopsies were performed 4.2 ± 1.3 h after death between 2004 and 2008 and samples were collected by 4 trained researchers, weekdays, weekends and holidays during the 5 year study period. Brains were examined macroscopically, sections were selected for light and electron microscopy, and frozen tissues collected. The general characteristics of the study population, including their cause of death are seen in Table 1 (Suppl). An average of 46 ± 11 olfactory bulb slides were examined per case. Paraffin embedded tissue was sectioned at a thickness of 7 μm and stained with hematoxylin and eosin (HE). Immunohistochemistry (IHC) was performed on serial sections as previously described (Calderón-Garcidueñas et al., 2008b). Antibodies included: β amyloid 17–24, 4G8 (Covance, Emeryville, CA 1: 1500), PHF-tau8 phosphorylated at Ser199–202-Thr205 (Innogenetics, Belgium, AT-8 1:1000), and α-synuclein phosphorylated at Ser-129, LB509 (In Vitrogen, Carlsbad, CA 1:1000). A number of brain tissues from all cases included in this work were previously blindly investigated for purposes of AD (Calderón-Garcidueñas et al., 2018). Olfactory bulbs were examined for AD and alpha-synucleinopathies hallmarks (Kovacs et al., 1999, 2001; Thal et al., 2002; Tsuboi et al., 2003; Braak et al., 2003, 2011a, 2011b, 2015, 2017; Del Tredici et al., 2002; Del Tredici and Braak, 2016; Attems et al., 2005, 2006, 2014; McKeith et al., 2005; Beach et al., 2009; Rüb et al., 2016). Tau pathology was scored using separate semiquantitative scores for neuropil threads (NTs) and neurofibrillary tangles (NFTs): 0 = absent, 0.5 = very mild (only single lesions), 1 = mild, 2 = moderate, and 3 = severe (Attems et al., 2005, 2006, 2014). The β- amyloid scoring was semiquantitative: 0 = absent, 1 = mild, few diffuse Aβ positive areas, no plaques, 2 = moderate, ≤ 3 plaques per high power field (HPF) x 200, and 3 = severe, 4 or more plaques HPF x 200 (Attems et al., 2014). Intracellular Aβ was scored 0 = absent and 1 = positive; vascular β- amyloid 0, 1,2 and 3 (severe). Alpha-synuclein was scored

as follows: 0 = absent, 1 = mild, few Lewy neurites, no Lewy bodies 2 = moderate, more than 1 Lewy body in a low power field (LPF), and sparce LNs; 3 = severe, > 1LBs and scattered LNs LPF and 4 very severe, numerous LBs and LNs (McKeith et al., 2005). Olfactory bulb tissue blocks were processed for EM with a focus on the neurovascular unit and the target organelles of CDNPs (González-Maciel et al., 2017). Genotyping for the presence of APOE alleles polymorphisms was done as previously described (Calderón-Garcidueñas et al., 2008b).

2.1.1. Air quality data

Metropolitan Mexico City residents are exposed year-round to fine particulate matter ($PM_{2.5}$) and ozone (O_3) concentrations above the United States National Air Ambient Quality Standards (NAAQS). For this autopsy study, we focused on < 2.5 μm particles and work with cumulative $PM_{2.5}$ ($CPM_{2.5}$) above the annual USEPA standard: 12 μg/m^3, reflecting lifetime exposures above the standard. Both, the $PM_{2.5}$ annual standard and the 24-h 35 μg/m^3 standard have been historically exceeded across the metropolitan area for the last 20 years (Bravo-Alvarez and Torres-Jardón, 2002; Marr et al., 2006; Querol et al., 2008; Aiken et al., 2009; Vega et al., 2010; Molina et al., 2010).

The accumulated burden of $PM_{2.5}$ for each subject-including pregnancy-was calculated based on their urban residency. Historical $PM_{2.5}$ levels were obtained from a combination of PM data from Mexico City Government Manual Monitoring Network for five representative urban sites: Tlalnepantla (NW), Xalostoc (NE), Pedregal (SW), Iztapalapa (SE) and Merced (downtown) (Fig. 1) and an approach considering the typical $PM_{2.5}/PM_{10}$ ratio for each of the representative sites. Historically, the highest $PM_{2.5}$ concentrations occur in the NE sector where intense industrial and traffic activities are prevalent and decrease towards the SW residential area.

Due that $PM_{2.5}$ concentrations were not measured regularly until 2004, the estimation procedure to obtain the $CPM_{2.5}$ before this year was based on the assumption that the trend of $PM_{2.5}/PM_{10}$ ratio obtained from the slopes of the correlations of these PM fractions in the period 2004–2010 represented the backward $PM_{2.5}/PM_{10}$ ratios trends for previous years. The results compared well with a number of $PM_{2.5}/PM_{10}$ ratios reported by academic groups in conference proceedings and published papers related to PM pollution in Mexico City in the 1980–2000 period (Bravo-Alvarez and Torres-Jardón, 2002; Vega et al., 2010; Molina et al., 2010). Then, the resulting ratios were used to estimate the $PM_{2.5}$ annual averages for each of the selected sites for the period 1989–2003. Since the study population included individuals older than 30 years at their time of death, we assumed a constant value for the $PM_{2.5}$ annual averages prior to 1989 equal to the annual mean for this year. Overall, the $PM_{2.5}/PM_{10}$ ratios were relatively constant ranging from ~ 0.45 in the Southwest towards ~ 0.25 in the Northeast. High $PM_{2.5}/PM_{10}$ ratios indicate a dominance of coarse particles in the PM_{10} while low ratios are associated to prevalence of fine particles.

With the estimated $PM_{2.5}$ annual averages for each site and year, we worked with a cumulative exposure function for fine particles ($CPM_{2.5}$) based on the assumption that the cumulated exposure to chronic levels of $PM_{2.5}$ above the respective USEPA NAAQS annual mean, averaged over 3 years of 12 μg/m^3, along the lifetime of each subject would have cumulative detrimental health effects on the individual. Also, we assumed that each subject spent most of the lifetime living in a specific area of the city.

Following the USEPA procedure to estimate the annual mean, we obtained a working annual average by averaging the 3 previous consecutive years, moving backwards in time up to 30 years starting in the base-year 2008. The resulting working annual average was used to obtain the $CPM_{2.5}$ for each of the individuals in the study, starting 1 year before their year of birth and up to the age of death (Table 1, Suppl). The working average data base was chosen according with the closest sampling site to their residence addresses during most of their

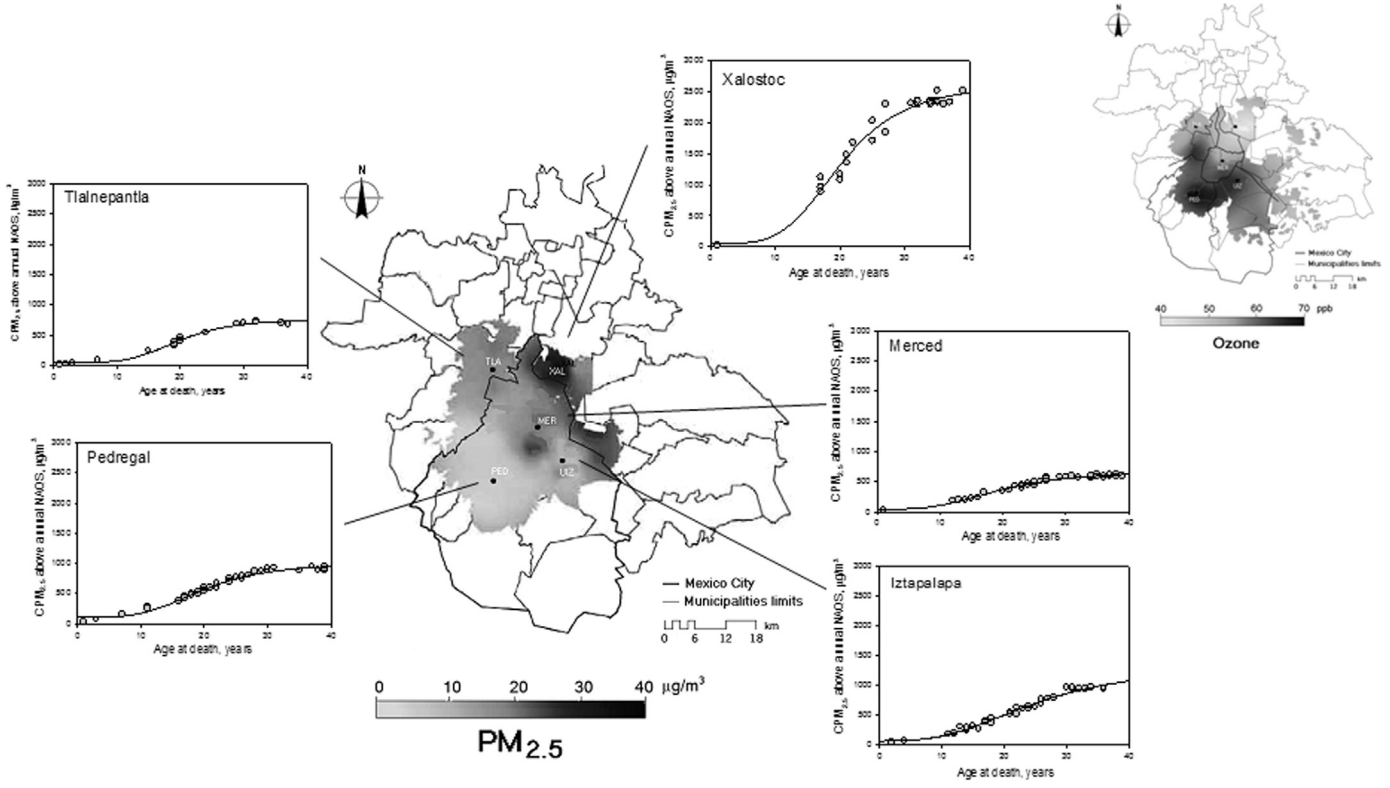

Fig. 1. Cumulated $PM_{2.5}$ trends of the annual, averaged over 3 years, mean concentrations in excess the USAEPA standard for 179 individuals according to their age at the time of death and residential location. The regressions are overlapped on a map showing the spatial distribution of the annual $PM_{2.5}$ concentrations for the base year 2008 (the last year of the 5 year study). The map in the upper right corner shows the spatial distribution of the annual average of the daily ozone 8-h maximum for 2008.

life.

Chemical PM composition studies in Mexico City have shown that the proportion of the different component PM species has not changed significantly along the years (Bravo-Alvarez and Torres-Jardón, 2002; Vega et al., 2010; Molina et al., 2010; Aiken et al., 2009; Marr et al., 2006; Querol et al., 2008). The $PM_{2.5}/PM_{10}$ ratio variations and the PM chemical composition are dependent on the site location and on the season. Typically, the coarse PM in MMC is strongly dominated by geological material ($SiO_2 + CO_2^{-3} + Al_2O_3 + Ca + Fe + Mg + K$) from dust resuspension. Organic and carbonaceous aerosols are the dominant species in the PM fine fraction. Particle emissions from gasoline and Liquefied Petroleum Gas Combustion (LPG) are dominated by organic carbonaceous aerosols (OC), while in diesel particles, black carbon (BC) is the main component (Molina et al., 2010). Organic aerosols in the air include primary hydrocarbon-like compounds, oxygenated organic compounds mostly secondary, organics from biomass burning, and small contributions of nitrogen-containing organics of primary combustion (Aiken et al., 2009). Also, critical for the brain effects, BC concentrations in $PM_{2.5}$ have not shown a decrease through the years (Aiken et al., 2009). BC is associated with polycyclic aromatic compounds (PAHs), semi-volatile species resulting from incomplete combustion of carbonaceous fuels such as gasoline and diesel vehicle exhaust gases (Marr et al., 2006). Most of PAHs in MMC are present in $PM_{2.5.}$ Trace metals in fine particles include Zn, Cu, Pb, Ti, Sn, Ba, Mn, Sb, V, Se, As, Ni, Cd, Cr in that order (Querol et al., 2008). Zn, Cu, Ba, Pb, and Cd are tracers of road traffic, while V and Ni are tracers of industrial emissions. Exposures to ozone (O_3) concentrations are also above the USEPA standards (annual fourth-highest daily maximum 8-h concentration, averaged over 3 years) all year long (Fig. 1). All other criteria pollutants for MMC, including nitrogen dioxide, sulfur dioxide and lead have shown elevated levels prior to 2000, but have been at or below the current EPA standards in the last 17 years.

2.2. Statistical analysis

Our sample size of 179 subjects was taken from a prior study of 203 subjects (Calderón-Garcidueñas et al., 2018) and it was defined a priori by sampling logistics in the 5 year study period balancing the expected results from previous neuropathology studies in young urbanites (Calderón-Garcidueñas et al., 2008b, 2011, 2017). We focused on summary statistics and graphical summary of the concerned staging variables: the major markers of Alzheimer and alpha-synucleinopathies (hTau, amyloid-β, α synuclein), age, gender, mode of death, and APOE status. Mode of death was analyzed in three major groups: accidents, homicides, and suicides. Subjects were divided by decades 1 and 2 (n: 57) and 3 and 4 (n: 122). Fig. 2 shows the comparison between the percentages of hTau pretangle and neurofibrillary tangles (NFT) stages in brain versus olfactory bulb hTau NTs, NFTs, and alpha-synuclein. Fig. 3 shows the amyloid-β (Aβ) phases in brain and OB Aβ plaques, vascular amyloid and intraneuronal amyloid. We also tested the relationship of the probability of committing suicide with respect to APOE status after adjusting age and CPM2.5 exposures. We identified APOE 4 carriers as individuals with higher suicide risk, and we performed logistic regression analysis to check if APOE 4 carriers had higher involvement of the targeted AD and alpha-synucleinopathies markers in the OB. Finally, we calculate cumulative incidence probabilities of developing moderate levels of the targeted variables against various amounts of cumulative PM2.5, and plotted those probabilities. We performed the statistical analyses using Excel and the statistical software 'R' (http://www.r-project.org/).

3. Results

Fig. 1 and Table 1 (Suppl) show the annual mean averages of $CPM_{2.5}$ for each individual based on their residence within arbitrary centroids in each of the five selected sampling sites. An arbitrary polynomial regression of second degree was applied to the $CPM_{2.5}$ data for each site as an approach to facilitate the expected cumulated $PM_{2.5}$ in the empty years. The regressions were overlapped on a figure of the estimated spatial distribution of the annual average $PM_{2.5}$ concentrations in MMC for 2008. The insert in Fig. 1 shows the annual average of the daily ozone 8-h maximum for the same year.

The Chi-squared test with Yates' continuity correction gave the two-sided p-value of 0.0040 ($\chi^2 = 8.2763$, d.f. $= (2-1) \times (2-1) = 1$) showing that the percentage of APOE 4 in the suicide group (28.1%) is indeed significantly higher than combined accident and homicide groups (8.2%).

In a model where $CPM_{2.5}$, age and APOE status were included as suicide predictors, having an APOE4 significantly increased the odds of dying by suicide 4.57 times ($p = 0.0025$), and 13.1, 10.3, 9.8, 9.4 and 6.3 times higher odds of OB vascular amyloid, neuronal amyloid accumulation, α Syn, hTau NFTs and NTs (all $p < 0.0001$) respectively, versus APOE4 non-carriers having similar $CPM_{2.5}$ exposure and age. The probability of developing moderate hTau in the entire cohort increases with $CPM_{2.5}$ ($\sim 1000\ \mu g/m^3$), however it did not reach statistical significance (p value = 0.0743).

The earliest immunohistochemical findings in children were hTau threads and neurites (NTs) followed by Lewy neurites (LNs) (Fig. 2). Amyloid plaques, mostly diffuse and few, were stationary throughout the four decades (Fig. 3), while amyloid neuronal accumulation and α-Syn (Fig. 2) increased with age. The causes of death are shown in Table 1 Suppl. It is noteworthy that suicide was a common cause of death in the mid20s age group.

3.1. Neuropathology

The hTau and β amyloid brains' scoring was done in a previous paper (Calderón-Garcidueñas et al., 2018). The olfactory bulb scoring for hTau NTs and NFTs, β amyloid, and α-synuclein and the brain scoring are seen in Table 1 Suppl.

3.2. First decade findings

The architecture of the OB layers in the 6 children ≤ 7y, was largely preserved. However, there were significant variations in the definition of the layers, particularly the mitral/tufted and the glomerular layers (Fig. 4A, B). In addition, the size and compactness of the glomeruli varied significantly among children (Fig. 4B, C, D, H). All six children were APOE 3/3 and all were classified in a previous work as pretangle stages a-c, 1a, 1b (Calderón-Garcidueñas et al., 2018), hTau threads were seen in 5/6 children ages 11 months to 7 years, and a 3 y old child had also vascular amyloid, Aβ42 immunoreactivity (IR) in neurons and glial cells around glomerular structures and diffuse amyloid positive areas (Fig. 4D, H). He also exhibited positive hTau and α-Syn IR (Fig. 4E–G). A two year old displayed isolated cells packed with particulate material (Fig. 4B Insert).

3.3. Second decade findings

Disorganization of the OB layers and small, irregular and loose glomeruli, some with areas of calcification were striking findings (Fig. 5A, B, C, K). The mitral cells were difficult to define in relation to granular cell layers (Fig. 5A, N). Severe disruption of the granule cell layer was present in teens (Fig. 5M, N). The vascular changes become striking, with prominent endothelial cells and thick walls, and extensive deposition of beta amyloid (Fig. 5A–C, F). We had 6 subjects ≤ 20 years, with nuclear hTau involving the glomerular layers and the anterior olfactory nucleus (Fig. 5O–Q), but very few hTau neurites in the AON (Fig. 5 INSERT Q) or elsewhere. Eight-six percent had hTau mostly as threads or as small tangles (50/57), while 77.2% have vascular amyloid (44/57), and 60% (34/57) had mild diffuse amyloid plaques. Interestingly, we had 5 teens with no IR to hTau that had

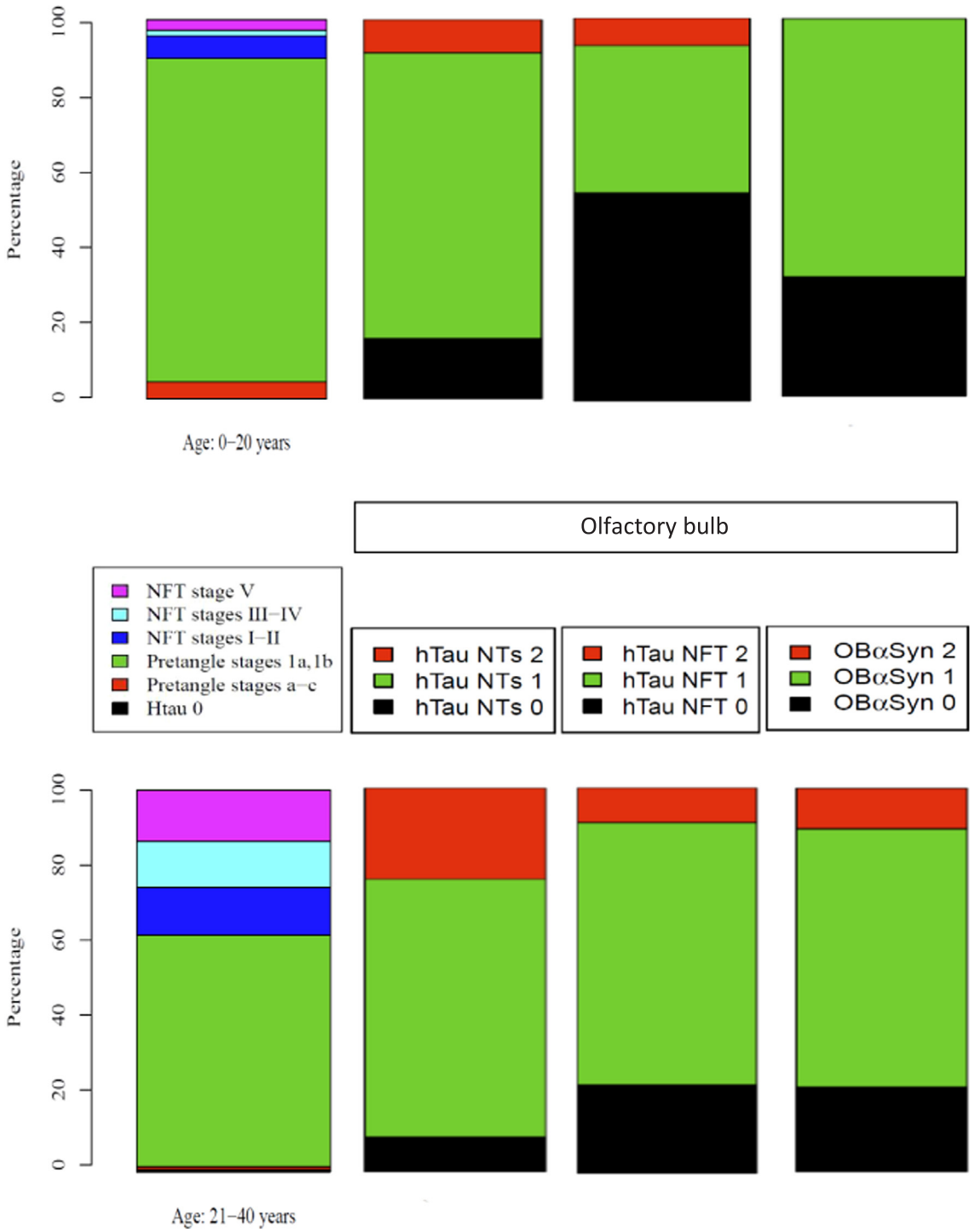

Fig. 2. Percentages of hTau stages (Braak and Del Tredeci, 2011, 2015; Braak et al., 2011) in subcortical and cortical stages in previous study (Htau Stage: 0 = absent, 1 = pretangle stages a-c, 2 = pretangle stages 1a, 1b, 3 = NFT stages I, II, 4 = NFT stages III–IV, 5 = NFT stages V–VI) (Calderón-Garcidueñas et al., 2018). Data compared to olfactory bulb percentages of hTau NTs (neurites) and NFTs (neurofibrillary tangles) (Htau scores NTs and NFTs separately: 0 = absent, 0.5 = very mild, only singly lesions, 1 = mild, 2 = moderate, 3 = severe) and α-synuclein (OB α-Syn) (Attems et al., 2005, 2006, 2014; McKeith et al., 2005) in the same subjects by age: 0–20 and 21–40 years at the time of death.

positive β amyloid either in blood vessels or neuronal. Lewy neurites and/or α-Syn aggregates in the somatodendritic compartment were seen in 76% (43/57) of cases. It is important to note, the anterior olfactory nucleus (AON) was rarely involved in the deposition of abnormal proteins other that increased IR to neuronal amyloid and/or nuclear hTau (Fig. 5Q, R). However, we saw subjects with significant obliteration of the AON by corporae amylacea (Fig. 5S). In this age group, we did not see amyloid plaques or α-Synuclein in the AON, nor we saw Lewy bodies anywhere. A clear example of the severity of the aggregated abnormal protein deposition was an 11 y old boy APOE3 (#7 in Table 1 Suppl), resident in a SW borough, showing extensive β-amyloid and alpha synuclein (Fig. 5D, E, F, T). The same child had accumulation of particulate matter in glomeruli neurons (Fig. 5H).

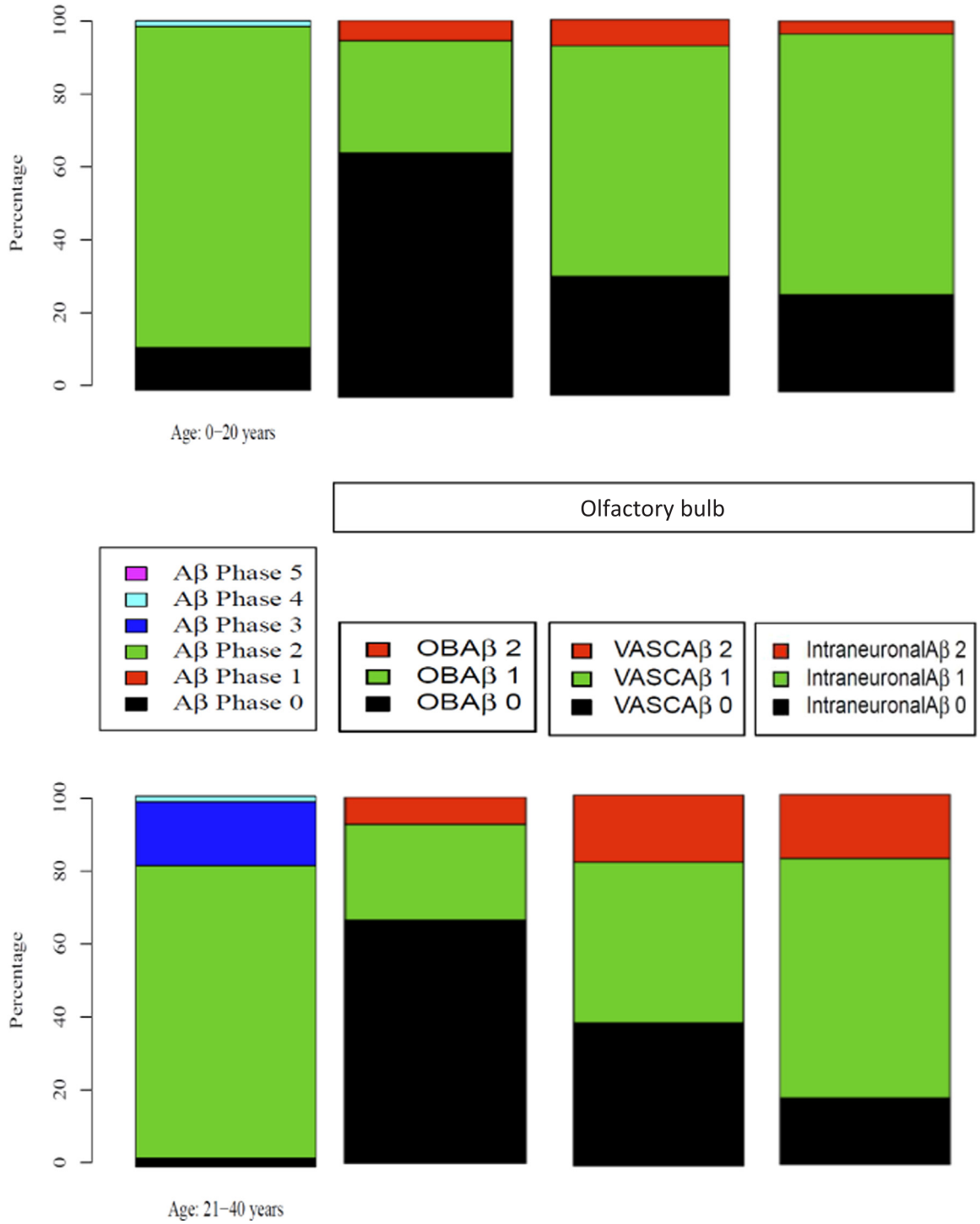

Fig. 3. Percentages of amyloid β phases in brain (Thal et al., 2002) (Brain Aβ Phase 0 = absent, 1 = basal temporal neocortex, 2 = all cerebral cortex, 3 = subcortical portions forebrain, 4 = mesencephalic components, 5 = Reticular formation and cerebellum). Data compared to olfactory bulb percentages of amyloid- β plaques (OBAβ: 0 = negative, 1 = mild few diffuse Aβ + areas NO Plaques, 2 = moderate ≤ 3 plaques HPF × 200, 3 = severe 4 or more plaques HPF × 200 (Attems et al., 2014). Vascular Aβ and Intraneuronal Aβ: 0 = absent, 1 = mild, 2 = moderate, 3 = severe.

3.4. Third and fourth decade findings

Striking findings included extensive deposition of corporae amylacea (CA) in subjects carrying an APOE 4 allele (Fig. 6A–D). Disorganization of the OB layers with few irregular and small glomeruli were striking findings (Fig. 6E). The anterior olfactory nucleus in many cases was occupied by massive amounts of CA (Fig. 6F). hTau neurites and NFTs can be seen in glomerular and granular cell layers and white matter tracts (Fig. 6G–I). Alpha-synuclein is seen as Lewy neurites and as aggregates in the somatodendritic compartment (Fig. 6J, K), but few distinguishable core-and-halo appearance Lewy bodies. Amyloid plaques, intracytoplasmic neuronal accumulation, and vascular amyloid pathology were frequent findings (Fig. 6L).

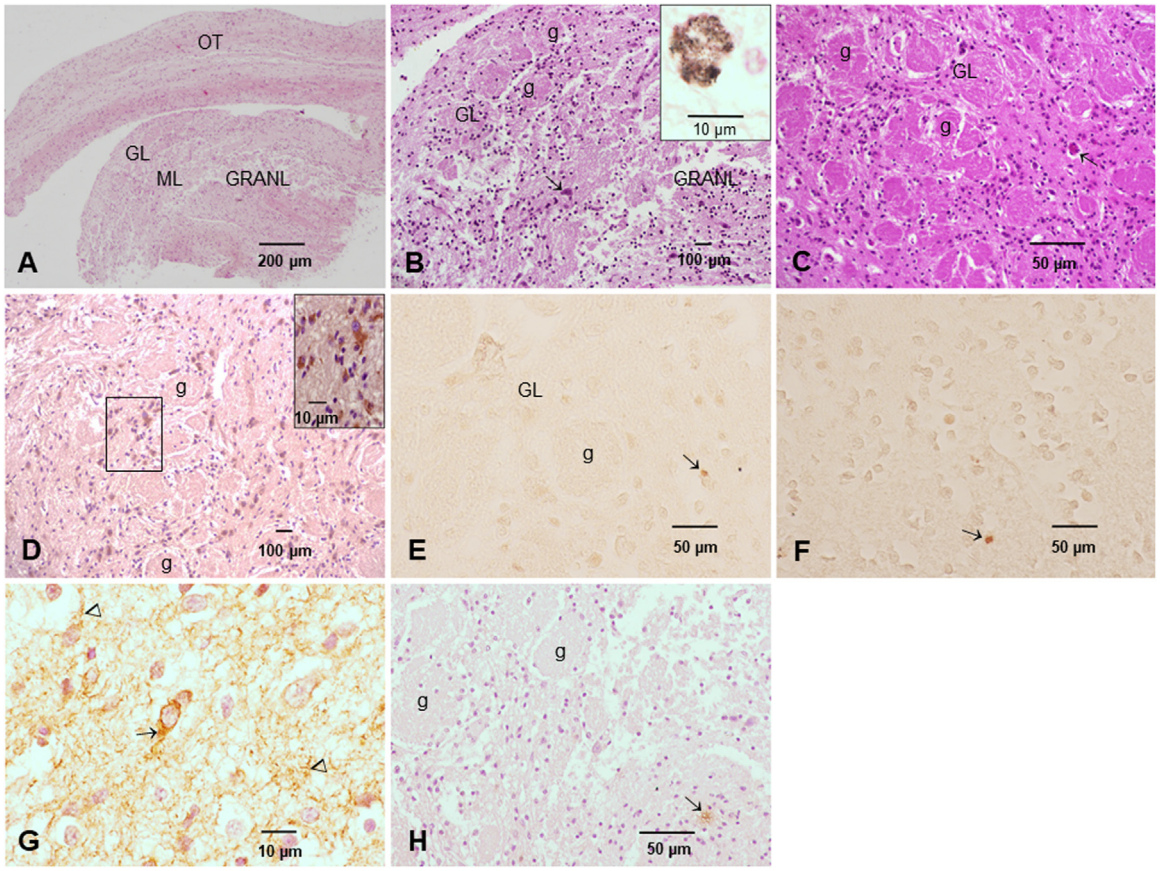

Fig. 4. Representative immunohistochemistry (IHC) and H&E sections from children in the first decade of life. A. Two year old male APOE 3/3, olfactory bulb 7 μm thick section. The anatomical organization of the olfactory bulb is still intact and the different layers could be defined: GL glomerular layer, ML mitral layer and GRANL granular cell layer. The olfactory tract (OT) is unremarkable. H&E, Scale bar 200 μm, B. Same child as A. Higher power shows focal disorganization of the OB architecture with isolated mitral neurons (arrow) H&E, Scale bar 100 μm. INSERT: Olfactory tract isolated cells showed abundant particulate material. H&E, Scale bar 10 μm, C. Three year old APOE 3/3. Glomeruli are abundant, with significant variation in size. Abnormal blood vessels with no visible lumen are seen throughout the sample (arrow). H&E, Scale bar 50 μm, D. Same child as C. Glomerular layer showed numerous immunoreactive (IR) amyloid β cells (brown product). IHC × Aβ counterstained with H, Scale bar 100 μm. INSERT: Higher power to show glomerular and periglomerular cells with cytoplasmic IR to Aβ. Scale bar 10 μm, E. Three year old APOE 3/3. Glomerular (g) region shows isolated hTau IR in axon initial segment (AIS) (arrow), contrasting with the negative background. IHC × AT8 without counterstain, Scale bar 40 μm, F. Three year old APOE 3/3. Granular cell layer, same child as E showing one hTau positive aggregated IR in axon initial segment (AIS). IHC × AT8 Scale bar 40 μm, G. Same child as C with α-Synuclein IR in glomerular region. Lewy neurites (arrowheads) are seen along α-Syn IR in neuronal bodies (short arrows). IHC × α-Syn phosphorylated at Ser-129, LB509, Scale bar 10 μm, H. An isolated glomerular immunoreactive (IR) area to amyloid β. ICH × Aβ, Scale bar 50 μm.

3.5. One micron toluidine blue sections and electron microscopy

One micron toluidine blue and electron microscopy findings were striking in relation to damage to unmyelinated and myelinated axons, and blood vessels with abnormal basement membranes in young children (Fig. 7A–D). Extensive accumulation of lipofuscin is seen in APOE 4 (Fig. 7C–E). The endothelial cell (EC) erythrophagocytosis was particularly prominent in APOE 4 children (Fig. 7G–I). Clusters of nanoparticles were common between red blood cells in capillaries (Fig. 7J, K). Children and teens also show significant accumulation of lipofuscin (Lf) in endothelial cells, pericytes, smooth muscle cells, and neurons. Abnormal neurovascular units were noted, and isolated beta pleaded sheet helicoidal conformation fibers (Fig. 7F) were observed along with CDNPs of sizes ranging from 9 to 60 nm. Extensive loss of unmyelinated and myelinated axons is seen in teens and young adults (Fig. 8A–C). The few surviving myelinated axons exhibit numerous CDNPs in their myelin sheets (Fig. 8A). CDNPs are seen within neurons and glial cells in target organelles including mitochondria, endoplasmic reticulum (ER), mitochondria-ER contacts (MERC) as well as in nuclear chromatin (Fig. 8B–J). CDNPs are present in damaged dendrites (Fig. 8H–J). The measurable size of the CDNPs were in the 9–60 nm range (average 19 ± 6 nm).

4. Discussion

Damage to the olfactory bulb (OB) in young Metropolitan Mexico City residents is early, progressive, exhibits Alzheimer and alpha-synucleinopathies hallmarks, and the damage is particularly severe in APOE 4 carriers. The neuropathology in children and teens strongly suggests the OB is an unavoidable target of pollution and nanoparticles likely play a critical role. The neurovascular unit (Iadecola, 2017) is an early, critical target and active endothelial phagocytosis of red blood cell (RBC) fragments containing combustion-derived nanoparticles (CDNPs) is an ongoing phenomenon. The significant vascular and extensive damage to unmyelinated and myelinated axons in the olfactory tracts and the hallmarks of the most prevalent tauopathies and synucleinopathies, obligates us to consider the olfactory bulb as a *sentinel* for evolving neurodegenerative processes. Strong support for teens and young adults olfactory testing is an expected outcome of this work.

The OB presence of β-amyloid, abnormal tau and α-synuclein pathology have been described in classic studies by a number of neuropathologists (Kovacs et al., 1999, 2001; Tsuboi et al., 2003; Braak et al., 2003, 2017; Del Tredici and Braak, 2016; Beach et al., 2009; Attems et al., 2005, 2006, 2014). The strong association of neurodegenerative OB pathology with olfaction deficits and targeted neuronal groups are

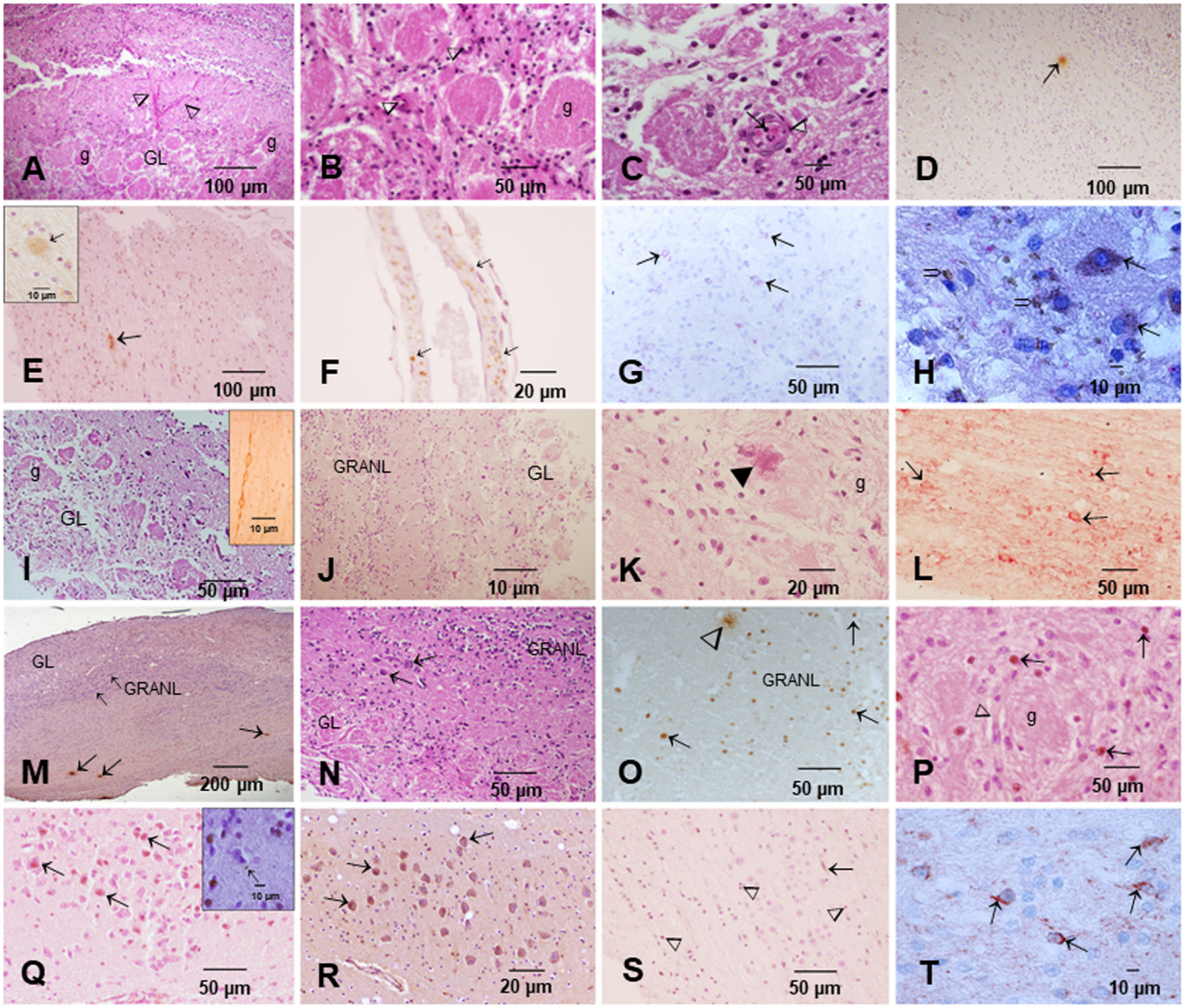

Fig. 5. Representative immunohistochemistry (IHC) and H&E sections from children and young adults in the second decade of life, A. Eleven year old boy APOE 3/3. The laminar organization of the olfactory bulb is still visible (glomerular layer, GL), but the different layers are ill-defined. There is significant variation in the glomeruli size (g) and blood vessels are prominently seen (arrowheads). H&E, Scale bar 100 μm, B. Around glomeruli (g) there are abnormal blood vessels with significant reduction in their lumen (arrowheads). H&E, Scale bar 50 μm, C. Same child as A and B with a higher power of the abnormal blood vessels in the glomerular region. Notice a polymorphonuclear leucocyte (arrow) attached to the vessel wall, and the vacuolated endothelial cells (arrowhead). H&E Scale bar 50 μm, D. Diffuse amyloid plaques are seen throughout the OB layers (arrow). IHC × Aβ counterstained with H, Scale bar 100 μm, E. Same child as A with extensive Aβ IR deposits of different sizes in the olfactory tract (arrow) IHC × Aβ counterstained with H, Scale bar 100 μm. INSERT: Discrete isolated diffuse Aβ plaque. Scale bar 10 μm, F. Aβ IR in medium arterial vessel in the subarachnoid space. Extensive deposits of amyloid in smooth muscle cells (arrows). IHC × Aβ counterstained with H. Scale bar 10 μm, G. Extensive α-Synuclein IR in glomerular region. IHC × α-Syn, LB509, red product, Scale bar 50 μm, H. The glomerular region is a target for accumulation of particulate material. Several cells within the glomerulus (short arrows) and outside are packed with particles (opened arrows). H&E, Scale bar 10 μm, I. Fourteen year old boy APOE 3/3 with striking variation in glomeruli size, some (g) are basically amorphous, without visible nuclei and very small and irregular. H&E, Scale bar 50 μm. INSERT: This child had moderate hTau neurites. IHC xAT8 Scale bar 10 μm, J. Seventeen year old boy APOE 3/3 with a significant abnormal laminar organization of the olfactory bulb and poor definition of the different layers (granular layer, GRANL left). The glomeruli layer (GL right side of the picture) shows very amorphous and pale glomeruli. H&E, Scale bar 10 μm, K. Same 17 y old boy as in I to show a glomerulus with an area of metaplastic calcification (black arrowhead). H&E, Scale bar 20 μm, L. Same teen as J, I. Extensive IR to α-synuclein (arrows). IHC x α-Syn, LB509, red product, Scale bar 50 μm, M. Twenty year old young man APOE 3/4. Numerous amyloid β diffuse plaques scattered throughout the specimen (arrows). Granular (GRANL) and glomerular layers (GL) are seen. IHC × Aβ counterstained with H, Scale bar 200 μm, N. Same subject as L. Severe disorganization of the laminar normal architecture with the glomerular region (GL) showing few and amorphous glomeruli, few clusters of mitral neurons (arrows) and a thin granular cell layer (GRANL). H&E, Scale bar 50 μm, O. APOE 3/4 male granular cell layer (GRANL). Nuclear hTau was extensive in this subject, few small hTau plaques (head arrow) are seen. IHC xAT8 Scale bar 50 μm, P. Same subject as N to show the glomerular region stained for hTau and counterstained with H. There is strong nuclear hTau IR (arrows). Notice the longitudinal segment of a blood vessel in close proximity to the central glomerulus (arrowhead). IHC xAT8 Scale bar 20 μm, Q. The anterior olfactory nucleus in this 20 y old male APOE 3/4 shows extensive nuclear hTau (arrows) but no IR NTs or NFTs. IHC xAT8 Scale bar 50 μm. INSERT: granular cell layer with both nuclear hTau and IR neurites (arrow), same subject. IHC xAT8 Scale bar 10 μm, R. Anterior olfactory nucleus in a 13 year old girl APOE 3/3. There is accumulation of amyloid β in the neuronal cytoplasm (arrows). IHC × Aβ Scale bar 20 μm, S. Anterior olfactory nucleus in an 11 year old showing corpora amylacea (arrowheads) and a few positive Aβ neuronal bodies (arrow). IHC × Aβ counterstained with H, Scale bar 50 μm, T. The same young man from Q shows extensive IR to α-synuclein in the glomerular layer. IHC × α-Syn, LB509, red product, Scale bar 10 μm.

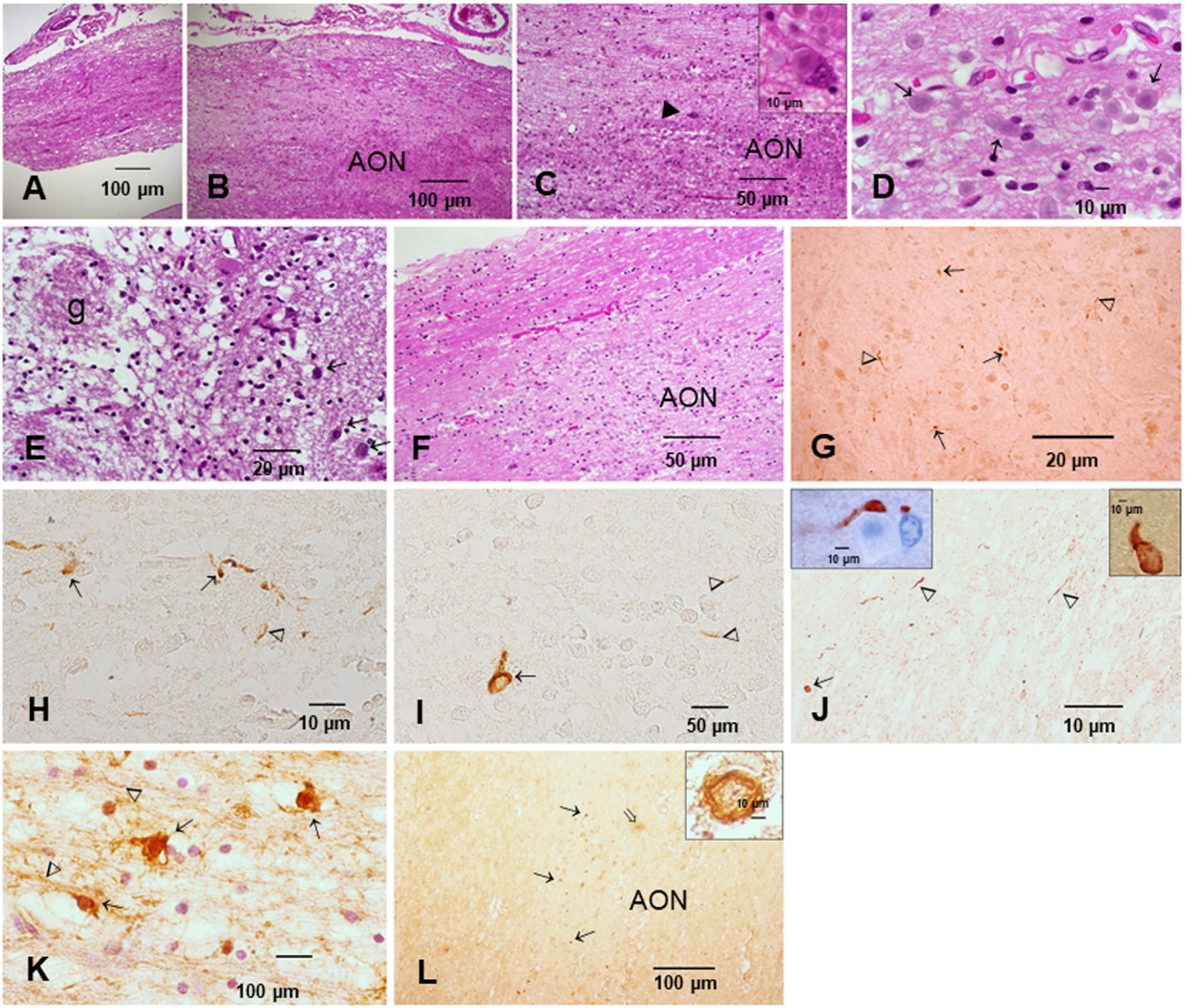

Fig. 6. Representative immunohistochemistry and H&E sections from subjects in the third and fourth decades of life. A. Thirty two year old female, APOE 4/4. Olfactory tracts of APOE4 carriers were characterized by extensive deposition of corpora amylacea (CA) and severe rarefaction of white matter tracts. H & E, Scale bar 100 μm, B. Same subject as A, olfactory bulb in the region of the anterior olfactory nucleus (AON), massively occupied by corpora amylacea. H & E, Scale bar 100 μm, C. Higher power of the AON area to show the corpora amylacea deposition and the presence of astrocytes with hyperchromatic, convoluted nuclei (arrowhead) containing CA in their cytoplasm (H&E Scale bar 50 μm). INSERT: abnormal astrocyte with large CA, note the abnormal surrounding neuropil. H&E Scale bar 10 μm, D. Close-up of corpora amylacea (CA). There is a wide spectrum of sizes and shapes corresponding to their orientation in the cutting plane (arrows). (H&E Scale bar 10 μm), E. APOE 4 carrier, the glomeruli (g) are very small and amorphous. A few mitral neurons remain (arrows). H&E Scale bar 50 μm, F. Twenty-five year old male, APOE 3/4, death by suicide, anterior olfactory nucleus AON occupied by corpora amylacea CA. H & E, Scale bar 50 μm, G. Forty year old male, APOE 3/3 moderate hTau NTs (arrowheads) and nuclear hTau (arrows) in glomerular layer IHC xAT8 Scale bar 20 μm, H. Thirty nine year old male, hTau NTs (arrows) and NFT (arrowhead) in granular layer IHC xAT8 Scale bar 10 μm, I. Same subject as G to show hTau NFTs (arrow) and NTs (arrowheads) in granular cell layer. IHC xAT8 Scale bar 10 μm, J. Twenty-eight year old female, APOE 3/4 (#106 in the Table 1 Suppl). Extensive IR α-synuclein LNs (arrowheads) and neuronal inclusions (arrow). IHC × α-Syn, LB509, brown product, Scale bar 50 μm. INSERT LEFT: Neuronal perikaryal inclusions are also seen. INSERT RIGHT: Enlarged IR neurites are common. Both inserts: IHC × α-Syn, LB509, red product, Scale bar 10 μm, K. Twenty-seven year old male, APOE 3/4 (#97 in the Table 1 Suppl). Neuronal perikaryal α-synuclein IR (arrows) and neurites(arrowheads). IHC × α-Syn, LB509, brown product, Scale bar 10 μm, L. Twenty-seven year old male, APOE 3/3 with a CPM2.5 of 2303 μg/m^3. Anterior olfactory nucleus, a few cells have IR to amyloid β (arrows) and an isolated diffuse amyloid plaque (arrowhead). IHC × Aβ counterstained with H, Scale bar 100 μm. INSERT: same subject, Aβ IR arteriole. Scale bar 10 μm.

also well documented (Segura et al., 2013; Ubeda-Bañon et al., 2014, 2017; Saiz-Sanchez et al., 2016; Doty, 2012; Woodward et al., 2017; Cave et al., 2016). A key concept in this discussion was put forward by Spires-Jones et al. (2017) "*Neurodegenerative diseases such as Alzheimer's disease, Lewy body disease (LBD), Parkinson's disease (PD) …have in common that protein aggregates represent pathological hallmark lesions*". We are indeed describing an overlap of hallmarks for AD, PD, LBD, etc., in megacity residents, suggesting that in the setting of air pollution, common etiopathology denominators are present.

Alzheimer's pathology in the olfactory bulb is present in the majority of patients with neuropathologically confirmed AD (Attems et al., 2014). In Attems et al., study of 536 autopsies (232 controls) with a mean age of 81.3 ± 0.46 years, 33.8% had a confirmed AD diagnosis. The AD cases showed OB hTau in 98. 3%, 51.7% had Aβ and 34.4% α-

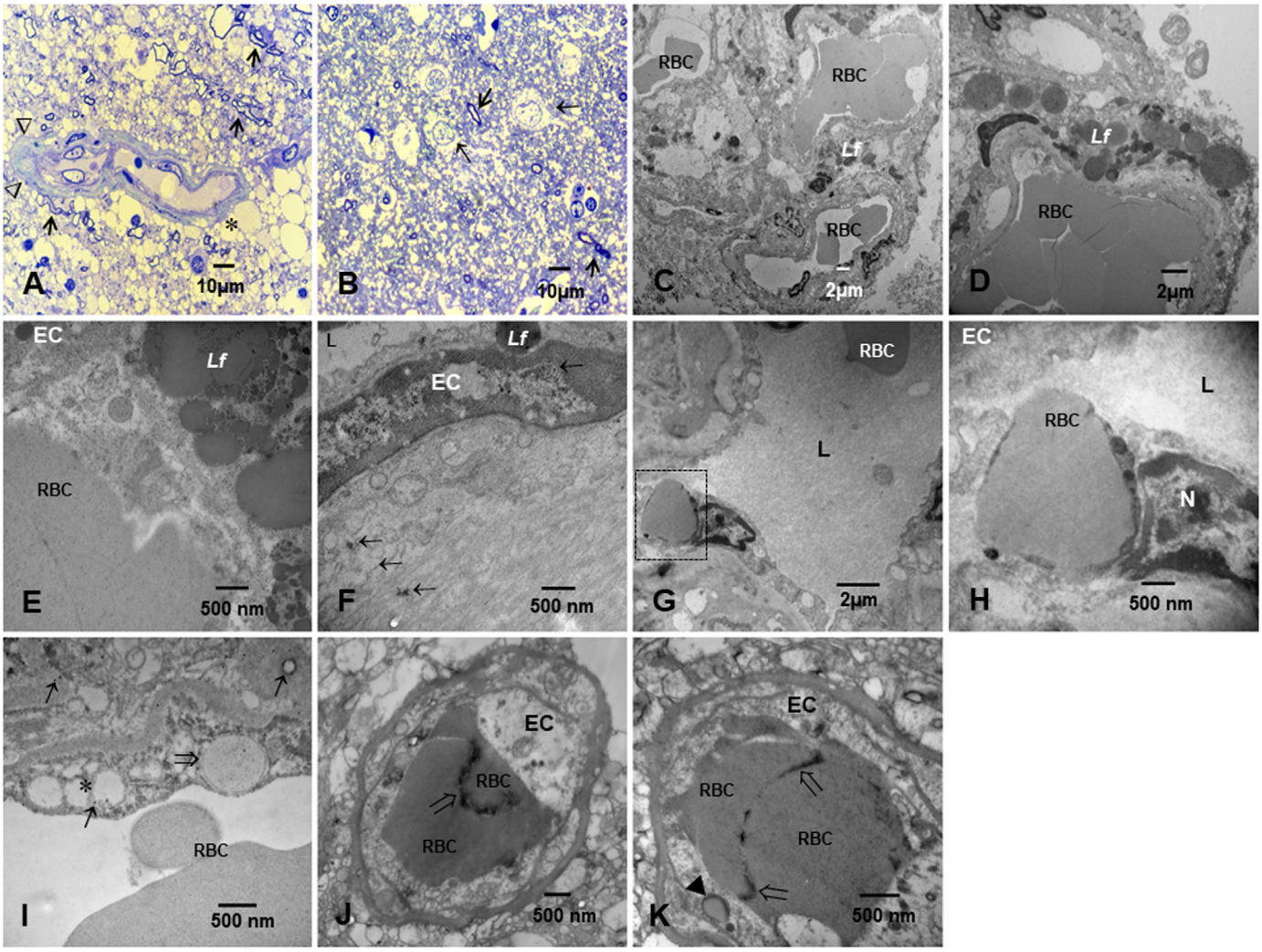

Fig. 7. Representative 1 μm toluidine blue and electron micrographs pictures. A. Fourteen year old girl APOE 3/3. Blood vessel basement membranes are focally thick (arrowhead), mild enlargement of the Virchow-Robin space (*) is noted and there is a significant loss of both myelinated (arrows) and unmyelinated axons. Toluidine blue, Scale bar 10 μm, B. Same 14 year old as A, section of mitral tufted cell layer. Few small myelinated axons remain and unmyelinated axons are difficult to identify. Small clusters of thin myelinated axons marked by short arrows and mitral neurons by longer arrows. Toluidine blue, 1 μm thick section. Scale bar 10 μm, C. Olfactory bulb in a 17 year old male APOE 3/3. Numerous lipofuscin (Lf) granules are seen. Red blood cells in the lumen of the vessels are marked RBC. Scale bar 2 μm, D. A close-up of a cluster of lipofuscin granules in the cytoplasm of an endothelial cell. Scale bar 200 nm, E. Endothelial cells exhibit extensive deposit of lipofuscin and RBC are in close contact with endothelial cells (EC). Scale bar 500 nm, F. Fourth teen year old girl with beta pleaded sheet helicoidal conformation fibers in the cytoplasm of an endothelial cell (EC) (lower half of the picture). Numerous CDNPs are seen in the EC nucleus and in the EC cytoplasm (arrows). Lf marks lipofuscin in close contact with the nucleus of the endothelial cell. Scale bar 500 nm, G. Seventeen year old male APOE 3/4. The endothelial cells of small blood vessels are involved in active erytrophagocitosis (square frame). Scale bar 2 μm, H. A close-up shows the square frame from G: one red blood cell (RBC) is surrounded by a membranous lysosomal structure in an endothelial cell (EC). The nucleus (N) of the EC is closed to the lysosomal structure. Scale bar 500 nm, I. Same 17 y old subject as C. The endothelial cell is phagocytizing a cellular non-identified fragment also containing numerous NPs (opened arrow). NPs are marked with arrows. The * marks apparently empty EC vacuoles. RBC are seen in the lumen of the vessel. Scale bar 500 nm, J. Capillaries are commonly occupied with red blood cells (RBC) containing significant amounts of NPs that orient themselves in a line between them (opened arrow). Scale bar 500 nm, K. A capillary in a 15 year old male. The NPs are also seen mostly between 2 RBC (opened arrows). Interestingly, a lipofuscin (Lf) early granule in the endothelial cytoplasm (EC) shows a rim of NPs (black arrowhead). Scale bar 500 nm.

Syn pathology. In controls, hTau pathology was present in 47.1%, α-Syn in 28.6% and Aβ pathology in 3.5%. Clinically demented cases in Attems et al., work showed significantly higher OB hTau, Aβ and α-Syn scores than non-demented cases (Attems et al., 2014). In Tsuboi et al., work, anterior olfactory nucleus (AON) hTau pathology was absent in the lower Braak stages and progressively increased to a 100% involvement in stages V and VI (Tsuboi et al., 2003). hTau AON pathology was very rare in their 15 controls with no significant neurodegenerative pathology. In their LBD cases, 77% had α-Syn in the AON and α-Syn AON pathology was only rarely detected in the absence of concomitant hTau pathology. Tsuboi et al., also discussed that APOE4 correlated with the severity of tau pathology in the AON in a gene dose-dependent manner (Tsuboi et al., 2003).

In sharp contrast to the OB pathology described in advanced AD, LBD and older PD patients, MMC young residents exhibited hTau in the axon initial segment (AIS) and in neurites as the very first OB tract findings, followed by α-Syn neurites in the glomerular and granular cell regions and the OB tracts. A striking finding –previously described (Calderón-Garcidueñas et al., 2018) in MMC exposed toddlers and teens in brainstem and supratentorial neurons, ependymal and endothelial cells- was the presence of nuclear hTau in glomerular and granular neurons and the AON in teens. The nuclear hTau would fail to efficiently protect DNA from oxidative stress as commented by Sultan et al., it will *contribute to functional failure of neurons early in life* (Sultan

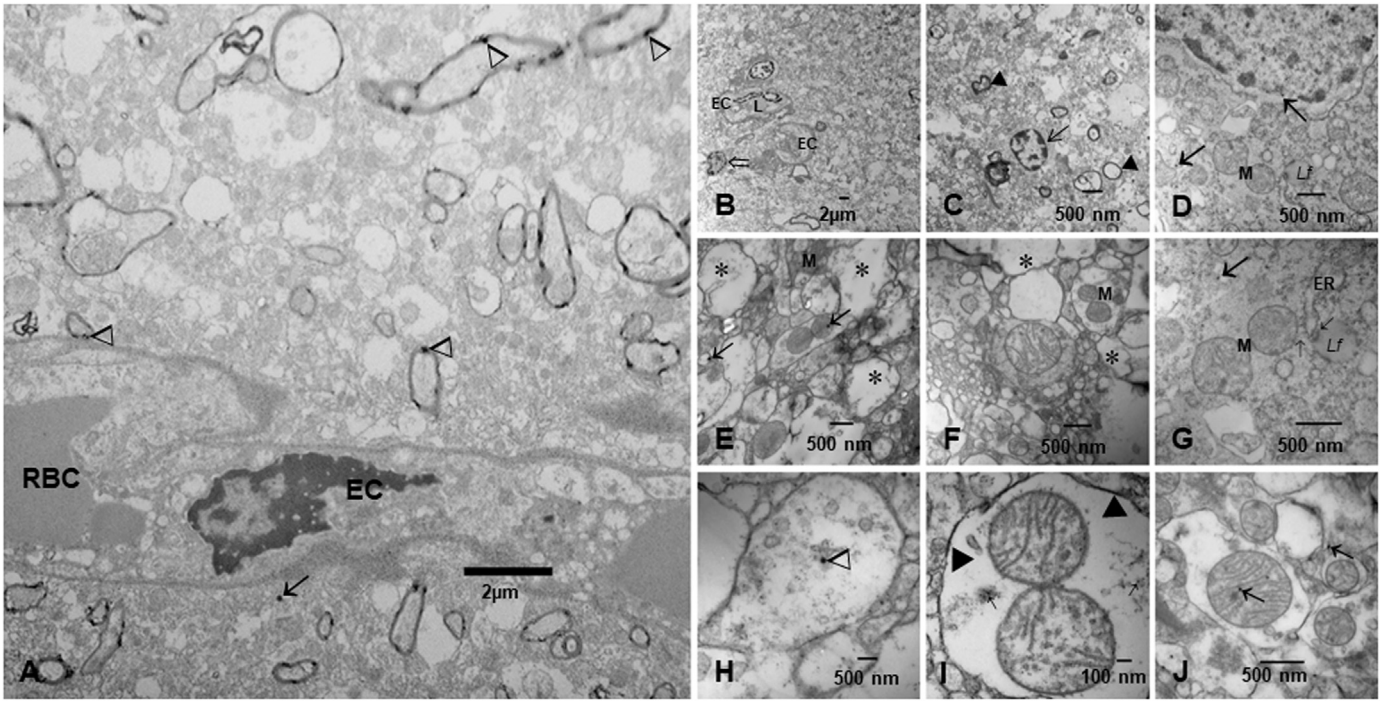

Fig. 8. Representative 1 μm toluidine blue and electron micrographs pictures, A. Fourteen year old girl APOE 3/3 medium size blood vessel in lower portion of picture (endothelial cell EC and red blood cells in lumen RBC). Several myelinated axons of different caliber, all show focal fragmentation of myelin and clusters of particles (arrowheads). One isolated combustion-derived nanoparticle cluster is marked (arrow). Scale bar 2 μm, B. Twenty-four year old male APOE 3/3. Capillaries with hyperplastic endothelial cells (EC) are surrounded by a glial cell (arrowhead). Lumen in a blood vessel is marked L. Scale bar 2 μm, C. Same subject, an oligodendrocyte (arrow) is surrounded by a few abnormal myelinated axons, some with very thin myelin (arrowhead, lower right). Scale bar 2 μm, D. A close-up of the oligodendrocyte to show abnormal nuclear membrane pores and NPs inside the nucleus (upper arrow). NPs are also present in the cytoplasm (lower left arrow) and mitochondria are marked (M). Lipofuscin granules are also present in the cytoplasm (Lf). Scale bar 500 nm, E. Unmyelinated axons with CDNPs in between axons and inside mitochondria (arrows). Damaged axons are marked with an *. Scale bar 500 nm, F. A common observation was the presence of severely damaged axons in close proximity to each other (*). Mitochondria are marked M. Scale bar 500 nm, G. The relationship between dilated endoplasmic reticulum (ER) and an early lysosomal (Lf) structure. The short arrow points to the space between the ER and the Lf. The lower arrow points to the proximity between mitochondria and ER. The larger upper right arrow points to a CDNP. Scale bar 500 nm, H. Severely damaged unmyelinated axon, the arrowhead points to a CDNP. Scale bar 2 μm, I. A common finding in between unmyelinated axons was the presence of nanoparticles (arrowheads), as well as inside the degenerating dendrite (arrows). Scale bar 100 nm, J. Twenty year old male APOE 3/3. Mitochondria in unmyelinated axons contain combustion-derived nanoparticles (central arrow). CDNPs are also seen outside mitochondria (right arrow). Scale bar 500 nm.

et al., 2011). The issue of early DNA damage in olfactory tissues (Calderón-Garcidueñas et al., 2003) is critical given the work of Omais and collaborators: *aberrant cell cycle reentry in post-mitotic neurons due to loss of cell cycle suppression ….as well as DNA damage can anticipate the development of neurodegenerative lesions and protein aggregates* (Omais et al., 2018).

The Aβ pathology in the form of diffuse plaques was mostly mild and remained stable throughout the first 4 decades of life. It is important to emphasize that the AON was not involved by hTau and/or α-Syn pathology in the first 4 decades; strikingly however, was the significant increase in AON corpora amylacea (CA), particularly in APOE4 carriers.

Corpora amylacea (CA) -glycoprotein-based deposition- in significant numbers is an outstanding OB finding (Pirici et al., 2014). In the work of Pirici et al., the three-dimensional structure of CA is complex with branching exhibiting a direct correlation with the diameter of vessels, while perivascular CAs are enclosed in pockets of the basement membranes. Interestingly, endogenous astrocytic heme oxygenase-1 (HO-1)-a cytoprotective enzyme-, reported to be localized in mitochondria under stress and contributing to preserve mitochondrial function, promotes transformation of normal mitochondria to CA-like inclusions (Song et al., 2014).

The work by Pisa et al. (2016) could be very relevant for this OB work. Pisa et al., showed the presence of CA immunoreactive- at their external surface- to fungal proteins in AD brain samples. In sharp contrast, CA from control brain tissue was almost devoid of fungal immunoreactivity (Pisa et al., 2016). Pisa' work is intriguing because when we look into the bioaerosol tracers in particulate matter, endotoxins from gram negative bacteria and tracers for fungal spores (fungal glucans, arabitol and mannitol) are indeed ubiquitous in outdoor, indoor and occupational scenarios (Rathnayake et al., 2016; Liu et al., 2016; Piecková, 2012; Heldal et al., 2003). Meteorological parameters including temperature, relative humidity, wind speed, and precipitation exhibited a substantial influence on the atmospheric concentrations of fungal aerosols and relate to non-haze and haze days (Priyamyada et al., 2017; Gao et al., 2014). Thus, living in a polluted atmosphere with endotoxins and fungae (or being in an occupational setting where bioaerosols are produced) adds to the OB expected pathology. Thus, several potential CA production pathways could be at work in OBs exposed to hostile conditions. Since the study subjects are young, age certainly is not a factor, in consequence other conditions have to be at play (Rohn, 2015; Augé et al., 2017).

A key finding was the accelerated OB pathology course relative to Braak early subcortical stages a-c, cortical lesions stages 1a, 1b, I and II and NFT stages (Braak and Del Tredeci, 2015). Thus in the first two decades when the majority of children and teens exhibited pretangle stages 1a and 1b, 84% have already OB hTau NTs (Fig. 2), strongly suggesting olfactory deficits could be an early guide of subcortical and cortical AD pretangle hTau (Braak et al., 2011b). α-Syn is a different story. We previously found LNs in the brainstem and the enteric nervous system (ENS) in children (Calderón-Garcidueñas et al., 2011, 2017) which coincided with 68% OB α-Syn neurites in the first two

decades. MMC children would be at Lewy pathology stages 1 and 2 according with the distribution of Lewy pathology in sporadic Parkinson's disease in Del Tredeci and Braak's work (2017). This PD staging would be critical because autonomic symptomatology occurs in > 60% of the young adult MMC population ages 20.5 ± 1.08 (Personal communication: Nora Vacaseydel-Aceves and Samuel C. Luévano-Castro, April 9, 2018).

The α-Syn OB location is important given the work of the Neuroplasticity and Neurodegeneration Laboratory at the University of Castilla-La Mancha and the Ecole Polytechnique Fédérale de Lausanne (Ubeda-Bañon et al., 2014, 2017; Saiz-Sanchez et al., 2016; Markram et al., 2004). Axons of sensory olfactory cells synapse with apical dendrites of mitral and tufted cells – the principal projection cells of the OB – within the glomeruli. Interneurons constitute 20–30% of the neuronal OB population, mostly granule or periglomerular cells (Saiz-Sanchez et al., 2016). These regions are precisely the location of the first Lewy neurites we observed in MMC youngsters, while the tertiary structures are not yet involved. Tertiary olfactory-recipient structures (van Hartevelt and Kringelbach, 2012) including the AON in their bulbar, intrapeduncular and retrobulbar portions are significantly involved in late PD, LBD and AD (Pearce et al., 1995; Del Tredici et al., 2002; Hubbard et al., 2007; Ubeda-Bañon et al., 2017).

A key element of vasopathology in the OB is the endothelial engagement in erythrophagocytosis (Fens et al., 2012). The circulating RBCs are innate carriers tolerating millions of nanoparticles under experimental conditions, and having biocompatibility, low immunogenicity, flexibility, and long systemic circulation (Pan et al., 2016; Villa et al., 2017; Han et al., 2018). RBC are exposed to oxidative stress related to iron containing magnetite nanoparticles (Calderón-Garcidueñas et al., 2007b; Yarjanli et al., 2017) with the detrimental combination of high redox activity, surface charge, and strongly magnetic behavior. Experimentally, RBC carrying NPs can get in close proximity to the endothelial surface and binding takes place, this is very important in highly exposed air pollution residents because endothelium adhesion efficiency of RBCs increases with their enhanced phosphatidylserine exposure (Yang et al., 2010; Fullstone et al., 2016; D'Apolito et al., 2016). To complicate matters, the phosphatidylserine exposure by RBCs is a powerful signal that initiates their phagocytic removal from circulation, a process that normally takes place in liver and spleen. Fens and collaborators discussed a very similar scenario to the polluted one. When they exposed their RBC to oxidative stress, erythrophagocitosis was a common event with the resultant cytotoxicity (Fens et al., 2012). Fens et al., suggested and we fully agreed "*significant erythrophagocitosis can induce endothelial cell loss….*" and a major damage to the OBs neurovascular unit. Why is this issue very relevant to city dwellers? Because odor stimulation induces capillary vascular responses that according to Chaigneau et al., are odorant and glomerulus-specific in rats (Chaigneau et al., 2003). Thus, since the responses will either increase or decrease RBC flow and in turn proper capillary vascular responses relate to synaptic activation, abnormal RBC and sticky endothelium will have detrimental effects on glomeruli synaptic activation.

Since nanoparticles are ubiquitous in OBs, factors related to access and transportation of NPs and aggregation and propagation of abnormal proteins in the OB and elsewhere in the CNS and ENS are important (Alvarez et al., 2013; Min et al., 2013; Wang et al., 2016; Xie et al., 2016; Sintov et al., 2016; Septiadi et al., 2018; Bourquin et al., 2018; Everett et al., 2018). Size, shape, surface charge and chemistry, chemical and biocorona composition, and solubility of NPs will be important for their degree of cytotoxicity and genotoxicity, their capacity to cause damage to target organelles and to produce aggregation and propagation of abnormal proteins in nervous tissues. The number of nanoparticles in ambient air can be very high; e.g., Rönkkö et al. (2017) described that even the smallest nanoparticles, called nanocluster aerosol particles, emitted by road transportation (1.3–3.0 nm) can contribute more than 50% to the ambient air particle number concentration. The deposition of such NCA as well as other NPs is high in the upper respiratory tract due to their diffusion movement, which ought to be of great concern for OBs damage (and CNS) (Rönkkö et al., 2017). Sintov et al. (2016) summarize three pathways involved in the transport of NPs through the OB i. axonal transport, ii. transcellular transport across the supporting cells in the olfactory region, iii. paracellular diffusion between supporting and neural cells. In the work of Wang et al., 2016, 35–50 nm Fe2O3 NPs instilled intranasally, were readily located by TEM in the axons of olfactory neurons and in mitochondria and lysosomes of hippocampus cells in exposed mice. In the work of Alvarez et al., 2013, gold NPs produced a strong acceleration of α-synuclein aggregation, the effects were dependent on the NPs size and concentration, being strongest for NPs 10 nm in diameter, which produced a 3-fold increase in the overall aggregation rate at concentrations as low as 20 nM. Since the NPs identified in Mexico City residents are iron highly magnetic NPs (Maher et al., 2016) the work of Xie et al., 2016, describing oxidative stress, lipid peroxidation and depletion of superoxide dismutase (SOD), glutathione, and catalase (CAT) activities upon iron oxide NPs exposures is very relevant to OBs damage. An additional factor of great interest would be *magnetic fields*. Min et al. (2013) argue that the rate of iron NP uptake and transport across cell monolayers is enhanced by a pulsed magnetic field and significantly inhibited at low temperature under both constant and pulsed magnetic field conditions, consistent with an active mechanism such as endocytosis, mediating NP transport. Thus, *environmental exposures to pulsed magnetic fields* could be another factor in the equation to compare *transport and damage* of iron oxide NPs across populations.

We have described different sizes of NPs in different neural regions both in humans and dogs, *so size matters* (González-Maciel et al., 2017; Calderón-Garcidueñas et al., 2007b, 2017, 2018). In the current OB study measurable NPs were in the range of 9–60 nm, thus included sizes ~ 10 nm, very efficient in α-synuclein aggregation (Alvarez et al., 2013).

The relationship between APOE4 status, suicide risk, depression, olfaction deficits, and cumulative $PM_{2.5}$ deserves extensive research. We found APOE4 carriers have 4.57 times higher suicide odds, and higher odds of OB AD and α Syn pathology. These findings are critical for several reasons: i. We fully expect a relationship between the OB neuropathology and olfactory deficits, a relationship that is clear in older populations with both AD and alpha-synucleinopathies (Kovacs et al., 2001; Tsuboi et al., 2003; Attems et al., 2005, 2014; Doty, 2012; Jellinger, 2009) ii. There are a significant number of papers on depression, OB size, and emotions (Negoias et al., 2010; Rottstaedt et al., 2018; Soudry et al., 2011; Oral et al., 2013; Chen et al., 2018). Misiak and collaborators stated that APOE4 is a key player in olfactory impairment and along with neuroimaging, psychological tools and molecular studies, holds promise for characterization of preclinical stages in people at risk (Misiak et al., 2017). We fully agreed.

> *The key question is how many young subjects with olfaction deficits, depression and altered emotional responses are already in their way to AD, PD/DLB?*

Finally, there is an issue we are obligated to discuss: what is the ultimate importance of the OB neuropathology spectrum in young highly exposed individuals and without any significant extraneural pathology? There is clear evidence of neurovascular unit damage with increased lipofuscin (Lf) as a striking finding. Lf formation is driven by ROS, is an intralysosomal, non-degradable, auto-fluorescent macromolecule which under physiological circumstances accumulates with age and can affect autophagy - the lysosomal degradation of a cell's constituents (McElnea et al., 2014). McElnea and collaborators make a statement that is applicable to the OB in exposed air pollution populations: *intracellular lipofuscin accumulation may have important effects on autophagy*. Indeed, Lf relates to the rate of oxidative damage to proteins, the functionality of mitochondrial repair systems, the impairment of proteasomal systems, and the functionality and effectiveness of the

lysosomes (Jung et al., 2007; Höhn et al., 2013). The issue of the autophagy-lysosome pathway (ALP) regulating intracellular homeostasis of the cytosolic protein SNCA/alpha-synuclein has been discussed by Minakaki et al. (2018). Inhibition of the ALP increases fused multivesicular body-autophagosome compartments and the "*autophagosome-exosome-like*" profile and alters the intracellular homeostasis of the cytosolic protein SNCA/alpha-synuclein. Why is Minakaki et al., outstanding work relevant to us? Because is precisely this autophagy-lysosome pathway that is impaired in alpha-synucleinopathies, including PD and DLB. Moreover, iron promotes α-Syn aggregation and transmission (Xiao et al., 2018). Xiao and collaborators' data demonstrated that iron promoted α-synuclein aggregation and transmission by *inhibiting autophagosome-lysosome fusion*. Further, Fe decreased the expression of nuclear transcription factor EB, a transcriptional regulator of autophagosome-lysosome fusion, and inhibited its nuclear translocation through activating AKT/mTORC1 signaling (Xiao et al., 2018). Thus, we have a distinct plausible pathway for α-synuclein aggregation and transmission (Xiao et al., 2018).

There is no question we have seen AD and PD/DLB olfactory bulb hallmarks, along with increased lipofuscin and corpora amylacea. This overlap is what we see as neuropathologists in a demented patient or in a presumably cognitively intact elderly *controls*. Braak and Del Tredeci commented about the spectrum of Lewy Body diseases and the fact cognitive impairment precede dementia in sporadic PD patients (Braak and Del Tredici, 2017). Also there is plenty of literature about the overlap between vascular disease and tautopathies and alpha synucleinopathies and the impact of vascular risk factors upon PD dementia and dementia with Lewy Bodies versus AD (Sweeney et al., 2018; Custodio et al., 2017; Nucera and Hachinski, 2018; Hilal et al., 2017). Love and Miners (2016) commented on a major contributor to the progressive hypoperfusion seen in AD: endothelin-1 (ET-1)- a marker of endothelial damage significantly increased in Mexico City children. ET-1 levels in MC children are positively strongly correlated with daily outdoor hours, and 7-day cumulative levels of PM air pollution < 2.5 μm (Calderón-Garcidueñas et al., 2007a, 2008a). Thus, within the context of ET-1 vasoconstriction and the neurovascular unit damage, both increased cerebrovascular resistance and loss of neural-mediated vasoreactivity could also play a role in the hypoperfusion effects (Yew and Nation, 2017; Nizari et al., 2017).

Our findings have several limitations: there is an overrepresentation of males, thus we are unable to discuss how the OB pathology progresses in females. Since we had no means of assessing olfactory and neurological data, their direct association with OBs pathology is not possible. This lack may have led to relevant olfactory, psychiatric, behavioral, and neurotoxic exposure information. On the other hand, based on our clinical studies we know about the olfaction deficits, their relationship with metabolic brain changes, the extensive cognitive deficits, their systemic inflammation, endothelial dysfunction, etc., in comparable *healthy* populations (Calderón-Garcidueñas et al., 2007a, 2008a, 2010).

We strongly support a complex overlap of tautopathies and alpha-synucleinopathies evolving from childhood with a common denominator: combustion-derived nanoparticles including atmospheric nanocluster aerosols (Maher et al., 2016; Rönkkö et al., 2017). Since the olfactory bulb is an early target and hTau is a prime actor, olfactory testing should be done along with early cognitive and behavioral testing to identify subjects at high neurodegenerative risk. APOE 4 carriers should start neuroprotective interventions in the first two decades of life.

A key challenge is to define clinical, laboratory, imaging, and cognitive *non-invasive* markers for the initial stages of the evolving complex tautopathies and alpha-synucleinopathies. It is imperative that we understand the earliest neuropathological changes upon exposures to air pollutants, the complexity of the interaction between sources and characteristics of pollutants and the ultimate CNS manifestations which will vary with age, nutritional, metabolic and genetic interactions.

Early interventions should be integrated in health and educational agendas along with identifying early gender-specific risk trajectories. We are certain air pollution should be included as an early risk factor in the research priorities to reduce global burden of dementia, ignoring the work of researchers across the globe and not supporting air pollution/early neurodegeneration prevention research, is not in the best interest of millions of exposed people. Pollution control should be prioritized, and supporting research related to air pollution and pediatric, teens and young adults neurodegenerative impact ought to be a goal in our prevention efforts to stop these diseases. Screening for olfaction deficits early in life, certainly in the first 2 decades of life would help to define cohorts at highest risk and provide mechanistic insights into major neurodegenerative fatal diseases including Alzheimer and Parkinson's. Preventive medicine ought to be our goal and we must consider the ramifications of lifelong air pollutant exposures on children and do what we can to protect them.

Contributors

LCG had access to all the data in the study, in charge of the study concept and design, oversaw the project, took part in the collection of the data, did the immunohistochemistry, review the electron micrographs, staged all cases, draft the manuscript and wrote the final manuscript. She takes responsibility for the integrity of the data and the accuracy of the data analysis. AGM and RRR participated in acquisition, analysis and interpretation of data, oversaw the project, did the electron microscopy job, took the EM pictures, review the electron micrographs, staged all cases, and contributed to the final manuscript. RJK review the entire project, wrote the final manuscript and provided critical revisions for important intellectual content. PSM provided statistical advice on the protocol, performed all the statistical analysis, wrote the final manuscript and provided critical revisions for important intellectual content. RTJ analyzed the pollutant data, made air pollution figures and wrote the pollution sections. TR contributed his expertise to the nanoparticle discussion, wrote the final manuscript and provided critical revisions for important intellectual content. RLD participated in interpretation of data, drafting of the manuscript, wrote the final manuscript and provided critical revisions for important intellectual content.

Declaration of interests

All authors declare no competing interests.

Funding

This research did not receive any specific grant from funding agencies in the public, commercial, or not-for-profit sectors.

Appendix A. Supplementary material

Supplementary data associated with this article can be found in the online version at http://dx.doi.org/10.1016/j.envres.2018.06.027.

References

Aiken, A.C., Salcedo, D., Cubison, M.J., et al., 2009. Mexico City aerosol analysis during MILAGRO using high resolution aerosol mass spectrometry at the urban supersite (T0) – Part 1: fine particle composition and organic source apportionment. Atmos. Chem. Phys. 9, 6633–6653.

Alvarez, Y.D., Fauerbach, J.A., Pellegrotti, J.V., et al., 2013. Influence of gold nanoparticles on the kinetics of α-synuclein aggregation. Nano Lett. 13, 6156–6163.

Attems, J., Lintner, F., Jellinger, K.A., 2005. Olfactory involvement in aging and Alzheimer's disease: an autopsy study. J. Alzheimers Dis. 7, 149–157.

Attems, J., Jellinger, K.A., 2006. Olfactory tau pathology in Alzheimer's disease and mild cognitive impairment. Clin. Neuropathol. 25, 265–271.

Attems, J., Walker, L., Jellinger, K.A., 2014. Olfactory bulb involvement in neurodegenerative diseases. Acta Neuropathol. 127, 459–475.

Augé, E., Cabezón, I., Pelegrí, C., Vilaplana, J., 2017. New perspectives on corpora amylacea in the human brain. Sci. Rep. http://dx.doi.org/10.1038/srep41807.
Beach, T.G., White 3rd, C.L., Hladik, C.L., et al., 2009. Olfactory bulb alpha-synucleinopathy has high specificity and sensitivity for Lewy body disorders. Acta Neuropathol. 117, 169–174.
Bourquin, J., Milosevic, A., Hauser, D., et al., 2018. Biodistribution, clearance, and long-term fate of clinically relevant nanomaterials. Adv. Mater. http://dx.doi.org/10.1002/adma.201704307.
Braak, H., Del Tredici, K., Rüb, U., et al., 2003. Staging of brain pathology related to sporadic Parkinson's disease. Neurobiol. Aging 24, 197–211.
Braak, H., Del Tredici, K., 2017. Neuropathological staging of brain pathology in sporadic Parkinson's disease: separating the wheat from the chaff. J. Park. Dis. 7, S73–S87.
Braak, H., Del Tredici, K., 2011a. The pathological process underlying Alzheimer's disease in individuals under thirty. Acta Neuropathol. 121, 171–181.
Braak, H., Thal, D.R., Ghebremedhin, E., Del Tredeci, K., 2011b. Stages of the pathological process in Alzheimer disease: age categories from 1 to 100 years. J. Neuropathol. Exp. Neurol. 70, 960–969.
Braak, H., Del Tredeci, K., 2015. The preclinical phase of the pathological process underlying sporadic Alzheimer's disease. Brain 138, 2814–2833.
Bravo-Alvarez, H.R., Torres-Jardón, R.J., 2002. Air pollution levels and trends in the Mexico City metropolitan area. In: Fenn, M., Bauer, L., Hernández, T. (Eds.), Urban Air Pollution and Forests: Resources at Risk in the Mexico City Air Basin Ecological Studies. Springer-Verlag, New York, pp. 121–159.
Calderón-Garcidueñas, L., Azzarelli, B., Acuna, H., et al., 2002. Air pollution and brain damage. Toxicol. Pathol. 30, 373–389.
Calderón-Garcidueñas, L., Maronpot, R.R., Torres-Jardón, R., et al., 2003. DNA damage in nasal and brain tissues of canines exposed to air pollutants is associated with evidence of chronic brain inflammation and neurodegeneration. Toxicol. Pathol. 31, 524–538.
Calderón-Garcidueñas, L., Vincent, R., Mora-Tiscareño, A., et al., 2007a. Elevated plasma endothelin-1 and pulmonary arterial pressure in children exposed to air pollution. Environ. Health Perspect. 115, 1248–1253.
Calderón-Garcidueñas, L., Franco-Lira, M., Torres-Jardón, R., et al., 2007b. Pediatric respiratory and systemic effects of chronic air pollution exposure: nose, lung, heart, and brain pathology. Toxicol. Pathol. 35, 154–162.
Calderón-Garcidueñas, L., Villarreal-Calderón, R., Valencia-Salazar, G., et al., 2008a. Systemic inflammation, endothelial dysfunction, and activation in clinically healthy children exposed to air pollutants. Inhal. Toxicol. 20, 499–506.
Calderón-Garcidueñas, L., Solt, A.C., Henríquez-Roldán, C., et al., 2008b. Long-term air pollution exposure is associated with neuroinflammation, an altered innate immuneresponse, disruption of the blood-brain-barrier, ultrafine particulate deposition, and accumulation of amyloid beta-42 and alpha-synuclein in children and young adults. Toxicol. Pathol. 36, 289–310.
Calderón-Garcidueñas, L., Franco-Lira, M., Henríquez-Roldán, C., et al., 2010. Urban air pollution: influences on olfactory function and pathology in exposed children and young adults. Exp. Toxicol. Pathol. 62, 91–102.
Calderón-Garcidueñas, L., D'Angiulli, A., Kulesza, R.J., et al., 2011. Air pollution is associated with brainstem auditory nuclei pathology and delayed brainstem auditory evoked potentials. Int. J. Dev. Neurosci. 29, 365–375.
Calderón-Garcidueñas, L., Kavanaugh, M., Block, M., et al., 2012. Neuroinflammation, hyperphosphorylated tau, diffuse amyloid plaques, and down-regulation of the cellularprion protein in air pollution exposed children and young adults. J. Alzheimer Dis. 28, 93–107.
Calderón-Garcidueñas, L., Serrano-Sierra, A., Torres-Jardón, R., et al., 2013. The impact of environmental metals in young urbanites' brains. Exp. Toxicol. Pathol. 65, 503–511.
Calderón-Garcidueñas, L., Mora-Tiscareño, A., Franco-Lira, M., et al., 2015. Decreases in short term memory, IQ and altered brain metabolic ratios in urban Apolipoprotein ε4 children exposed to air pollution. APOE modulates children's brain air pollution responses. J. Alzheimers Dis. 45, 757–770.
Calderón-Garcidueñas, L., Reynoso-Robles, R., Vargas-Martínez, J., et al., 2016a. Prefrontal white matter pathology in air pollution exposed Mexico City Young urbanites and their potential impact on neurovascular unit dysfunction and the development of Alzheimer's disease. Environ. Res. 146, 404–417.
Calderón-Garcidueñas, L., Ávila-Ramírez, J., Calderón-Garcidueñas, A., et al., 2016b. Cerebrospinal fluid biomarkers in highly exposed $PM_{2.5}$ urbanites: the risk of Alzheimer's and Parkinson's diseases in young Mexico city residents. J. Alzheimers Dis. 54, 597–613.
Calderón-Garcidueñas, L., Reynoso-Robles, R., Pérez-Guillé, B., et al., 2017. Combustion derived nanoparticles, the neuroenteric system, cervical vagus, hyperphosphorilated alpha synuclein and tau in young Mexico City residents. Environ. Res. 159, 186–201.
Calderón-Garcidueñas, L., Gónzalez-Maciel, A., Reynoso-Robles, R., et al., 2018. Hallmarks of Alzheimer disease are evolving relentlessly in Metropolitan Mexico City infants, children and young adults. APOE4 carriers have higher suicide risk and higher odds of reaching NFT stage V at ≤ 40 years of age. Environ. Res. 164, 475–487.
Cave, J.W., Fujiwara, N., Weibman, A.R., Baker, H., 2016. Cytoarchitectural changes in the olfactory bulb of Parkinson's disease patients. NPJ Park. Dis. 2, 16011. http://dx.doi.org/10.1038/npjparkd.2016.11.
Chaigneau, E., Oheim, M., Audinat, E., Charpak, S., 2003. Two-photon imaging of capillary blood flow in olfactory bulb glomeruli. Proc. Natl. Acad. Sci. USA 100, 13081–13086.
Chen, H., Kwong, J.C., Copes, R., et al., 2017. Living near major roads and the incidence of dementia, Parkinson's disease, and multiple sclerosis: a population-based cohort study. Lancet 389, 718–726.
Chen, B., Zhong, X., Mai, N., et al., 2018. Cognitive impairment and structural abnormalities in late life depression with olfactory identification impairment: an Alzheimer's disease-like pattern. Int. J. Neuropsychopharmacol. http://dx.doi.org/10.1093/ijnp/pyy016.
Custodio, N., Montesinos, R., Lira, D., et al., 2017. Mixed dementia: a review of the evidence. Dement. Neuropsychol. 11, 364–370.
D'Apolito, R., Taraballi, F., Minardi, S., et al., 2016. Micro fluidic interactions between red blood cells and drug carriers by image analysis techniques. Med. Eng. Phys. 38, 17–23.
Del Tredici, K., Rüb, U., De Vos, R.A., et al., 2002. Where does Parkinson disease pathology begin in the brain? J. Neuropathol. Exp. Neurol. 61, 413–426.
Del Tredici, K., Braak, H., 2016. Review: sporadic Parkinson's disease: development and distribution of α-synuclein pathology. Neuropathol. Appl. Neurobiol. 42, 33–50.
Doty, R.L., 2008. The olfactory vector hypothesis of neurodegenerative disease: is it viable? Ann. Neurol. 63, 7–15.
Doty, R.L., 2012. Olfaction in Parkinson's disease and related disorders. Neurobiol. Dis. 46, 527–552.
Doty, R.L., 2017. Olfactory dysfunction in neurodegenerative diseases: is there a common pathological substrate? Lancet Neurol. 16, 478–488.
Enroth, J., Saarikoski, S., Niemi, J., et al., 2016. Chemical and physical characterization of traffic particles in four different highway environments in the Helsinki metropolitan area. Atmos. Chem. Phys. 16, 5497–5512.
Everett, J., Collingwood, J.F., Tiendana-Tjhin, V., et al., 2018. Nanoscale synchrotron X-ray speciation of iron and calcium compounds in amyloid plaque cores from Alzheimer's disease subjects. Nanoscale. http://dx.doi.org/10.1039/c7nr06794a.
Fens, M.H., van Wijk, R., Andringa, G., 2012. A role for activated endothelial cells in red blood cell clearance: implications for vasopathology. Haematologica 97, 500–508.
Fullstone, G., Nyberg, S., Tian, X., Battaglia, G., 2016. From the blood to the central nervous system: a nanoparticle's journey through the blood-brain barrier by transcytosis. Int. Rev. Neurobiol. 130, 41–72.
Gao, M., Qiu, T.L., Jia, R.Z., et al., 2014. Concentration and size distribution of bioaerosols at non-haze and haze days in Beijing. Huan Jing Ke Xue 35, 4415–4421.
González-Maciel, A., Reynoso-Robles, R., Torres-Jardón, R., et al., 2017. Combustion derived nanoparticles in key brain target cells and organelles in young urbanites: culprit hidden in plain sight in Alzheimer's disease development. J. Alzheimers Dis. 59, 189–208.
Han, X., Wang, C., Liu, Z., 2018. Red blood cells as smart delivery systems. Bioconjug. Chem. 29, 852–860.
Heldal, K.K., Halstensen, A.S., Thorn, J., et al., 2003. Upper airway inflammation in waste handlers exposed to bioaerosols. Occup. Environ. Med. 60, 444–450.
Hilal, S., Akoudad, S., van Duijn, C.M., et al., 2017. Plasma Amyloid-β levels, cerebral small vessel disease, and cognition: the Rotterdam study. J. Alzheimers Dis. 60, 977–987.
Höhn, A., Jung, T., Grune, T., 2013. Pathophysiological importance of aggregated damaged proteins. Free. Radic. Biol. Med. 71, 70–89.
Hubbard, P.S., Esiri, M.M., Reading, M., et al., 2007. Alpha-synuclein pathology in the olfactory pathways of dementia patients. J. Anat. 211, 117–124.
Iadecola, C., 2017. The neurovascular unit coming of age: a journey through neurovascular coupling in health and disease. Neuron 96, 17–42.
Jellinger, K.A., 2009. Olfactory bulb alpha-synucleinopathy has high specificity and sensitivity for Lewy body disorders. Acta Neuropathol. 117, 215–216.
Jung, T., Bader, N., Grune, T., 2007. Lipofuscin: formation, distribution, and metabolic consequences. Ann. NY Acad. Sci. 1119, 97–111.
Jung, C.R., Lin, Y.T., Hwang, B., 2015. Ozone, particulate matter, and newly diagnosed Alzheimer's disease: a population-based cohort study in Taiwan. J. Alzheimers Dis. 44, 573–584.
Kovacs, T., Cairns, N.J., Lantos, P.L., 1999. β amyloid deposition and neurofibrillary tangle formation in the olfactory bulb in ageing and Alzheimer's disease. Neuropathol. Appl. Neurobiol. 25 (4812-491).
Kovacs, T., Cairns, N.J., Lantos, P.L., 2001. Olfactory centres in Alzheimer's disease: olfactory bulb is involved in early Braak's stages. Neuroreport 12, 285–288.
Liu, F., Lai, S., Reinmuth-Selzle, K., et al., 2016. Metaproteomic analysis of atmospheric aerosol samples. Anal. Bioanal. Chem. 408, 6337–6348.
Love, S., Minres, J.S., 2016. Cerebrovascular disease in ageing and Alzheimer's disease. Acta Neuropathol. 131, 645–658.
Maher, B., Ahmed, I.A.M., Karloukovski, V., et al., 2016. Magnetite pollution nanoparticles in the human brain. Proc. Natl. Acad. Sci. USA 113, 10797–10801.
Marabotti, C., Piaggi, P., Scarsi, P., et al., 2017. Mortality for chronic-degenerative diseases in Tuscany: ecological study comparing neighboring areas with substantial differences in environmental pollution. Int. J. Occup. Med. Environ. Health 30, 641–653.
Markram, H., Toledo-Rodriguez, M., Wang, Y., et al., 2004. Interneurons of the neocortical inhibitory system. Nat. Rev. Neurosci. 5, 793–807.
Marr, L.C., Dzepina, K., Jimenez, J.L., et al., 2006. Sources and transformations of particle-bound polycyclic aromatic hydrocarbons in Mexico City. Atmos. Chem. Phys. 6, 1733–1745.
McElnea, E.M., Hughes, E., McGoldrick, A., et al., 2014. Lipofuscin accumulation and autophagy in glaucomatous human lamina cribrosa cells. BMC Ophthalmol. 14, 153.
McKeith, I.G., Dickson, D.W., Lowe, J., et al., 2005. Diagnosis and management of dementia with Lewy bodies: third report of the DLB Consortium. Neurology 65, 1863–1872.
Min, K.A., Shin, M.C., Yu, F., et al., 2013. Pulsed magnetic field improves the transport of iron oxide nanoparticles through cell barriers. ACS Nano 7, 2161–2171.
Minakaki, G., Menges, S., Kittel, A., et al., 2018. Autophagy inhibition promotes SNCA/alpha-synuclein release and transfer via extracellular vesicles with a hybrid autophagosome-exosome-like phenotype. Autophagy 15, 1–22.
Misiak, M.M., Hipolito, M.S., Ressom, H.W., et al., 2017. Apo E4 alleles and impaired

olfaction as predictors of Alzheimer's disease. Clin. Exp. Psychol (doi: 0.4172/2471-2701.1000169).
Molina, L.T., Madronich, S., Gaffney, J.S., et al., 2010. An overview of the MILAGRO 2006 Campaign: Mexico City emissions and their transport and transformation. Atmos. Chem. Phys. 10, 8697–8760.
Mylläri, F., Karjalainen, P., Taipale, R., et al., 2017. Physical and chemical characteristics of fuel-gas particles in a large pulverized fuel-fired power plant boiler during co-combustion of coal and wood pellets. Combust. Flame 176, 554–566.
Negoias, S., Croy, I., Gerber, J., et al., 2010. Reduced olfactory bulb volume and olfactory sensitivity in patients with acute major depression. Neuroscience 169, 415–421.
Nizari, S., Romero, I.A., Hawkes, C.A., 2017. The role of perivascular innervation and neurally mediated vasoreactivity in the pathophysiology of Alzheimer's disease. Clin. Sci. 131, 1207–1214.
Nucera, A., Hachinski, V., 2018. Cerebrovascular and Alzheimer disease: fellow travelers or partners in crime? J. Neurochem. 144, 513–516.
Omais, S., Jaafar, C., Ghanem, N., 2018. "Till Death Do Us Part": a potential irreversible link between aberrant cell cycle control and neurodegeneration in the adult olfactory bulb. Front. Neurosci. 12, 144. http://dx.doi.org/10.3389/fnins.2018.00144.
Oral, E., Aydin, M.D., Aydin, N., et al., 2013. How olfaction disorders can cause depression? The role of habenular degeneration. Neuroscience 240, 63–69.
Pan, D., Vargas-Morales, O., Zern, B., et al., 2016. The effect of polymeric nanoparticles on biocompatibility of carrier red blood cells. PLoS One 11 (3), e0152074.
Pearce, R.K., Hawkes, C.H., Daniel, S.E., 1995. The anterior olfactory nucleus in Parkinson's disease. Mov. Disord. 10, 283–287.
Piecková, E., 2012. Adverse health effects of indoor moulds. Arh. Hig. Rada. Toksikol. 63, 545–549.
Pisa, D., Alonso, R., Rábano, A., Carrasco, L., 2016. Corpora amylacea of brain tissue from neurodegenerative diseases are stained with specific antifungal antibodies. Front. Neurosci. http://dx.doi.org/10.3389/fnins.2016.00086.
Pirjola, L., Dittrich, A., Niemi, J.V., et al., 2016. Physical and chemical characterization of real-world particle number and mass emissions from city buses in Finland. Environ. Sci. Technol. 50, 294–304.
Pirici, I., Mărgăritescu, C., Mogoantă, L., et al., 2014. Corpora amylacea in the brain form highly branched three-dimensional lattices. Rom. J. Morphol. Embryol. 55, 1071–1077.
Priyamyada, H., Singh, R.K., Akila, M., et al., 2017. Seasonal variation of the dominant allergenic fungal aerosols-Oneyear study from southern Indian region. Sci. Rep. http://dx.doi.org/10.1038/s41598-017-11727-7.
Querol, X., Pey, J., Minguillón, M.C., et al., 2008. PM speciation and sources in Mexico during the MILAGRO-2006 Campaign. Atmos. Chem. Phys. 8, 111–121.
Rathnayake, C.M., Metwali, N., Baker, Z., 2016. Urban enhancement of PM10 bioaerosol tracers relative to background locations in the Midwestern United States. J. Geophys. Res. Atmos. 121, 5071–5089.
Rohn, T.T., 2015. Corpora Amylacea in neurodegenerative diseases: cause or effect? Int. J. Neurol. Neurother. 2 (3), 031.
Rönkkö, T., Pirjola, L., Ntziachristos, L., et al., 2014. Vehicle engines produce exhaust nanoparticles even when not fueled. Environ. Sci. Technol. 48, 2043–2050.
Rönkkö, T., Kuuluvainen, H., Karjalainen, P., et al., 2017. Traffic is a major source of atmospheric nanocluster aerosol. Proc. Natl. Acad. Sci. USA 114, 7549–7554.
Rottstaedt, F., Weidner, K., Strauß, T., et al., 2018. Size matters-The olfactory bulb as a marker for depression. J. Affect Disord. 229, 193–198.
Rüb, U., Stratmann, K., Heinsen, H., et al., 2016. The brainstem tau cytoskeletal pathology of Alzheimer's disease: a brief historical overview and description of its anatomical distribution pattern, evolutional features, pathogenetic and clinical relevance. Curr. Alzheimer Res. 13, 1178–1197.
Saiz-Sanchez, D., Flores-Cuadrado, A., Ubeda-Bañon, I., et al., 2016. Interneurons in the human olfactory system in Alzheimer's disease. Exp. Neurol. 276, 13–21.
Segura, B., Baggio, H.C., Solana, E., et al., 2013. Neuroanatomical correlates of olfactory loss in normal aged subjects. Behav. Brain Res. 246, 148–153.
Septiadi, D., Crippa, F., Moore, T.L., et al., 2018. Nanoparticle-cell interaction: a cell mechanics perspective. Adv. Mater. http://dx.doi.org/10.1002/adma.201704463.
Sintov, A.C., Velasco-Aguirre, C., Gallardo-Toledo, E., et al., 2016. Chapter Six - metal nanoparticles as targeted carriers circumventing the blood–brain barrier. In: Khuloud, T.A.-J. (Ed.), International Review of Neurobiology. Academic Press, London, pp. 199–227.
Song, W., Zukor, H., Liberman, A., et al., 2014. Astroglial heme oxygenase-1 and the origin of corpora amylacea in aging and degenerating neural tissues. Exp. Neurol. 254, 78–89.
Soudry, Y., Lemogne, C., Malinvaud, D., et al., 2011. Olfactory system and emotion: common substrates. Eur. Ann. Otorhinolaryngol. Head Neck Dis. 128, 18–23.
Spires-Jones, T.L., Attems, J., Thal, D.R., 2017. Interactions of pathological proteins in neurodegenerative diseases. Acta Neuropathol. 134, 187–205.
Sultan, A., Nesslany, F., Violet, M., et al., 2011. Nuclear tau, a key player in neuronal DNA protection. J. Biol. Chem. 286, 4566–4575.
Sweeney, M.D., Sagare, A.P., Zlokovic, B.V., 2018. Blood-brain barrier breakdown in Alzheimer disease and other neurodegenerative disorders. Nat. Rev. Neurol. 14, 133–150.
Thal, D.R., Rüb, U., Orantes, M., Braak, H., 2002. Phases of A beta-deposition in the human brain and its relevance for the development of AD. Neurology 58, 1791–1800.
Tsuboi, Y., Wszolek, Z.K., Graff-Radford, N.R., et al., 2003. Tau pathology in the olfactory bulb correlates with Braak stage, Lewy body pathology and apolipoprotein epsilon4. Neuropathol. Appl. Neurobiol. 29, 503–510.
Ubeda-Bañon, I., Saiz-Sanchez, D., de la Rosa-Prieto, C., Martinez-Marcos, A., 2014. α-Synuclein in the olfactory system in Parkinson's disease: role of neural connections on spreading pathology. Brain Struct. Funct. 219, 1513–1526.
Ubeda-Bañon, I., Flores-Cuadrado, A., Saiz-Sanchez, D., Martinez-Marcos, A., 2017. Differential Effects of Parkinson's Disease on Interneuron Subtypes within the Human Anterior Olfactory Nucleus. Front. Neuroanat. 11, 113. http://dx.doi.org/10.3389/fnana.2017.00113.
vanHartevelt, T.J., Kringelbach, M.I., 2012. The olfactory system. In: Mai, J.K., Paxinos, G. (Eds.), The Human Nervous System. Academic Press, London, pp. 1219–1238.
Vega, E., Eidels, S., Ruiz, H., et al., 2010. Particulate air pollution in Mexico City: a detailed view. Aerosol Air Qual. Res. 10, 193–211.
Villa, C.H., Cines, D.B., Siegel, D.L., Muzykantov, V., 2017. Erythrocytes as carriers for drug delivery in blood transfusion and beyond. Transfus. Med. Rev. 31, 26–35.
Wang, B., Wang, Q., Chen, H., et al., 2016. Size-dependent translocation pattern, chemical and biological transformation of nano-and submicron-sized ferric oxide particles in the central nervous system. J. Nanosci. Nanotechnol. 16, 5553–5561.
Woodward, M.R., Dwyer, M.G., Bergsland, N., et al., 2017. Olfactory identification deficit predicts white matter tract impairment in Alzheimer's disease. Psychiatry Res. 266, 90–95.
Xiao, Y., Chen, X., Huang, S., et al., 2018. Iron promotes α-synuclein aggregation and transmission by inhibiting TFEB-mediated autophagosome-lysosome fusion. J. Neurochem. 145, 34–50.
Xie, Y., Liu, D., Cai, C., et al., 2016. Size-dependent cytotoxicity of Fe3O4 nanoparticles induced by biphasic regulation of oxidative stress in different human hepatoma cells. Int. J. Nanomed. 11, 3557–3570.
Yang, Y., Koo, S., Lin, C.S., Neu, B., 2010. Specific binding of red blood cells to endothelial cells is regulated by non-adsorbing macromolecules. J. Biol. Chem. 285, 40489–40495. http://dx.doi.org/10.1074/jbc.M110.116608.
Yarjanli, Z., Ghaedi, K., Esmaeili, A., et al., 2017. Iron oxide nano particles may damage to the neural tissue through iron accumulation, oxidative stress, and protein aggregation. BMC Neurosci. 18, 51.
Yew, B., Nation, D.A., 2017. Alzheimer's disease neuroimaging initiative. Cerebrovascular resistance: effects on cognitive decline, cortical atrophy, and progression to dementia. Brain 140, 1987–2001.
Zhu, Y., Hinds, W., Kim, S., et al., 2002. Study of ultrafine particles near a major highway with heavy-duty diesel traffic. Atmos. Environ. 36, 4323–4335.